

# Multi-Agent Reinforcement Learning for Dynamic Routing Games: A Unified Paradigm

Zhenyu Shou<sup>a</sup>, Xuan Di<sup>a,b,\*</sup>

<sup>a</sup>*Department of Civil Engineering and Engineering Mechanics, Columbia University*

<sup>b</sup>*Data Science Institute, Columbia University*

---

## Abstract

This paper aims to develop a unified paradigm that models one’s learning behavior and the system’s equilibrating processes in a routing game among atomic selfish agents. Such a paradigm can assist policymakers in devising optimal operational and planning countermeasures under both normal and abnormal circumstances. To this end, a multi-agent reinforcement learning (MARL) paradigm is proposed in which each agent learns and updates her own en-route path choice policy while interacting with others on transportation networks. This paradigm is shown to generalize the classical notion of dynamic user equilibrium (DUE) to model-free and data-driven scenarios. We also illustrate that the equilibrium outcomes computed from our developed MARL paradigm coincide with DUE and dynamic system optimal (DSO), respectively, when rewards are set differently. In addition, with the goal to optimize some systematic objective (e.g., overall traffic condition) of city planners, we formulate a bilevel optimization problem with the upper level as city planners and the lower level as a multi-agent system where each rational and selfish traveler aims to minimize her travel cost. We employ the developed flow-dependent multi-agent deep Q learning approach on the lower level to solve for optimal route choices of travelers and a Bayesian optimization method on the upper level to solve for optimal controls by city planners. We demonstrate the effect of two administrative measures, namely tolling and signal control, on the behavior of travelers and show that the systematic objective of city planners can be optimized by a proper control. The results show that on the Braess network, the optimal toll charge on the central link is greater or equal to 25, with which the average travel time of selfish agents is minimized and the emergence of Braess paradox could be avoided. In a large-sized real-world road network with 69 nodes and 166 links, the optimal offset for signal control on Broadway is derived as 4 seconds, with which the average travel time of all controllable agents is minimized.

*Keywords:* Multi-Agent Reinforcement Learning (MARL), Dynamic Routing Games, Model-Based and Data-Driven, Bayesian Optimization (BO)

---

## 1. Introduction

With a growing number of drivers relying on GoogleMaps or other navigation tools for dynamic routing, one question of interest is that, when everybody follows the advisory of shortest paths provided by one central platform, will these drivers still be able to gain from taking these paths? This paper aims to tackle this question by accounting for competition among drivers. When one chooses a path dynamically while navigating a road network, others may also do so to compete for limited road resources. Therefore it is crucial to model the dynamic routing choices of many drivers simultaneously. To address the above problem, we will first review the literature on route choice of single-agent and then move to that of multi-agent.

### 1.1. Single-agent route choice

While traveling from an origin to a destination, one needs to select a sequence of road segments. Thus, en-route path choice is inherently a sequential decision-making process, in which at each junction

---

\*Corresponding author. Tel.: +1 212 853 0435;  
Email address: sharon.di@columbia.edu (Xuan Di)

one decides what the next link to take. Markov decision processes (MDP) (Puterman, 1994) and reinforcement learning (RL) (Sutton and Barto, 1998) have become popular tools to model such a sequential process, in which travelers are rational agents to optimize a prescribed objective function (or reward) (Seongmoon Kim et al., 2005; Kim et al., 2016). The assumption of rationality has been challenged by various behavioral and economic theories, including, to name a few, bounded rationality (Di et al., 2013; Di and Liu, 2016), prospect theory (Gao et al., 2010; Xu et al., 2011; Yang and Jiang, 2014; Zhang et al., 2018), and regret theory (de Moraes Ramos et al., 2011). In this paper we assume travelers are perfectly rational agents in the context of selfish routing. In other words, every traveler is a self-interest agent who aims to maximize individual accumulative rewards or minimize individual cost or maximize payoffs.

### 1.2. Multi-agent route choice

One’s route choice contributes marginally to traffic congestion on its picked route. Accordingly, travelers on a road network interact among one another while selecting routes collectively. When everybody optimizes her own rewards while others do so simultaneously, a routing (or congestion) game forms. Multi-agent selfish routing games have been studied using both prescriptive (i.e., what one ought to behave in route choice) and descriptive (i.e., how one actually select routes) approaches. Prescriptive approaches can be categorized as **model-based** because of its high reliance on models that prescribe route choice behaviors, while descriptive ones are categorized as **data-driven** being accountable for real-world routing data.

The most popular prescriptive models belong to the traffic assignment problem. The traffic assignment problem models one’s routing behavior while interacting with others in order to predict network-wide traffic congestion. Static traffic assignment is proposed for the long-term planning purpose, and dynamic traffic assignment (DTA) predicts dynamic traffic flow evolution in the short term by modeling one’s within-day route choice or/and departure-time choice (Friesz et al., 1989; Peeta and Ziliaskopoulos, 2001; Nie and Zhang, 2005). DTA integrates both notions of travel demand (consistent with static traffic assignment) and traffic flow (i.e., dynamic traffic evolution) and is thus appropriate for modeling dynamic movement of travelers across a network (Friesz et al., 2013). DTA typically consists of two components, namely a route choice (and/or departure time choice) model determining inflows to each link and a dynamic network loading model propagating traffic flows through the network (Bliemer et al., 2017; Yu et al., 2020). However, such a normative framework could be challenging to accommodate the substantive amount of trajectories of individual vehicles thanks to emerging technologies (e.g., GPS, mobile phones, and DSRC). It thus warrants a paradigm shift from model-based to data-based routing to leverage high-resolution trajectories, in order to better model one’s en-route adaptive behavior in a dynamic and competitive environment.

This motivates us to believe that multi-agent reinforcement learning (MARL) (Littman, 1994; Hu and Wellman, 1998) could be a promising direction for dynamic routing games with a large amount of interacting travelers on networks. Different from DUE that evolves traffic dynamics based on mathematical models (with which traffic state transitions and travel costs are computed), MARL based approaches simply let agents (i.e., drivers) interact with the road network and learn towards optimal policies, thus enjoying the flexibility of being model-free. Furthermore, thanks to the advancement of deep Q networks (Mnih et al., 2015), deep reinforcement learning (DRL) based approaches can now tackle a large-sized problem with a very large or even continuous state and action space. In summary, MARL is advantageous over the classical model-based DTA framework for its computational efficiency with a large amount of agents on large-sized road networks, modeling of en-route adaptive behaviors of individual agents, and taking one’s online travel experiences as input to dynamically update routing behaviors.

### 1.3. MARL and Multi-agent Markov game

As a game-theoretic framework for MARL, Markov game (Littman, 1994) is a generalization of MDPs to multiple interacting agents with competing goals, in which the environment makes transitions probabilistically in response to the agents’ actions. Markov game is typically defined as a non-cooperative game where self-interested agents aiming to maximize their own payoffs. In a Markov game, the solution concept of Nash equilibrium is generally adopted (Hu and Wellman, 1998). At a Nash equilibrium, one agent’s strategy (i.e., policy) is the best response to other agents’ strategy. MARL is an efficient and versatile tool to solve for the optimal policy of each agent. Among the pioneering studies, Littman (1994) proposes a minimax Q-learning algorithm to solve for the optimal policies of two agents with opposed goals in a zero-sum game, and Hu and Wellman (1998) extends it to a general-sum game and provided a multi-agent Q-learning algorithm.

Recent literature has witnessed various applications of MARL to high-dimensional and complicated tasks such as playing the game of Go (Silver et al., 2016, 2017), Poker (Brown and Sandholm, 2018, 2019), Dota 2 (OpenAI, 2018), and StarCraft II (Vinyals et al., 2019). Outside the computer game domain, MARL has also attracted significant attention and been used in energy sharing (Prasad and Dusparic, 2019), federated control (Kumar et al., 2017), and sequential social dilemma (Leibo et al., 2017), to name a few. Interested readers are referred to Nguyen et al. (2020) for a comprehensive review of applications and challenges of MARL. In the transportation domain, we have also seen a growing trend of applying MARL to vehicle routing (Bazzan and Klügl, 2008; Bazzan and Grunitzki, 2016), traffic signal control (Bakker et al., 2010; Chen et al., 2020), fleet management (Lin et al., 2018; Shou and Di, 2020), order dispatching (Li et al., 2019), and autonomous driving (Palanisamy, 2019; Bhalla et al., 2020). However, its application to dynamic routing game is still at its nascent stage.

#### 1.4. Literature on reinforcement learning based route choices

The existing literature on dynamic routing games using RL-based approaches is listed in Table 1. Based on how to define the action of an agent, we broadly categorize RL-based route choice models into two groups. In the first group, the action of an agent is a route (Zhou et al., 2020; Ramos et al., 2018; Stefanello et al., 2016). For example, in Ramos et al. (2018); Stefanello et al. (2016), for an agent aiming to go to her destination node from her origin node, the action space for her is the  $k$  shortest paths from her origin to her destination. These studies assume that every driver does follow her chosen route until she reaches her destination. In reality, however, drivers could deviate from their chosen route when they realize that traffic condition on some alternative routes might be better, especially when they get stuck in traffic on the current route. To capture this en-route adaptive behavior of drivers, the second group of studies focus on en-route traffic assignment, or route choice from the perspective of a driver. In these studies, the action space of an agent currently at a node is the outbound links from the node (Grunitzki et al., 2014; Bazzan and Grunitzki, 2016; Mao and Shen, 2018). In other words, every agent needs to decide which outbound link to choose whenever the agent arrives at a node, until the agent reaches some terminal node. This en-route decision-making process captures the adaptive behavior of real drivers.

To study the en-route decision-making process of drivers, both single-agent RL and multi-agent RL are used in the literature. A single-agent Q-learning approach is developed in Mao and Shen (2018) with the use of some global information such as congestion status in the definition of state. The authors bootstrapped two traffic profiles from the PeMS dataset and derived an optimal policy for the agent. Unfortunately, single-agent RL fails to capture the competition among adaptive agents. Multi-agent RL is recently used to tackle the multi-driver route choice task (Grunitzki et al., 2014; Bazzan and Grunitzki, 2016). Despite of modeling multi-driver interactions, these studies use independent multi-agent tabular Q-learning where every agent is treated as an independent learner who has no information of other agents.

A key issue arises when independent learners treat other agents as part of the stochastic environment, that is, theoretical convergence guarantee for Q-learning does not hold, because the environment is no longer Markovian and stationary (Matignon et al., 2012; Nguyen et al., 2018). To fill this research gap, we develop a flow-dependent multi-agent deep Q-learning approach which captures the interaction among adaptive agents via a flow-dependent mean action. The flow-dependent mean action is defined as the traffic flow on the chosen link right after an agent enters the link. The use of the flow-dependent mean action not only captures the competition among agents, but also enables Q-value sharing and policy sharing, which is computationally favorable, especially in a large-sized problem with multi-commodity multi-class agents.

Noticing that in a road network, in addition to the infrastructure supply (i.e., road resources) and travelers (i.e., traffic demand), there is another player, that is, city planner, who can impact the behavior of travelers. With selfish and rational travelers aiming to minimize their travel cost, city planners can achieve some systematic goal by imposing externalities on individuals' cost via various operational measures such as congestion pricing or traffic signal control. Therefore, we formulate such interactions between travelers and city planners as a bilevel optimization task. We employ the developed flow-dependent multi-agent deep Q learning approach on the lower level to solve for optimal route choices of travelers and a Bayesian optimization scheme on the upper level to solve for optimal controls by city planners.

Table 1: Existing research on dynamic routing using RL based approaches

Research type	Reference	Setting	State	Action set	Reward	Algorithm	Bilevel optimization	Gap
Route-based	Stefanello et al. (2016)	Multi-agent	-	$k$ shortest routes from origin to destination	Negative time	travel Independent tabular Q-learning	No	-
	Ramos et al. (2018)	Multi-agent	-	$k$ shortest routes from origin to destination (anticipating disutility)	App-based regret (anticipating disutility)	Independent tabular Q-learning	No	-
	Zhou et al. (2020)	Multi-agent	-	Feasible routes from origin to destination	Negative time	travel Bush-Mosteller RL scheme	No	-
	Grunitzki et al. (2014)	Multi-agent	(node)	Outbound links	Negative time (Individual and systematic)	travel Independent tabular Q-learning	No	Independent learning suffers from non-stationary and non-Markovian issues;
	Bazzan and Grunitzki (2016)	Multi-agent	(node)	Outbound links	Negative time	travel Independent tabular Q-learning	No	tabular Q-learning could not handle continuous or large state/action space
En-route	Mao and Shen (2018)	Single-agent	(time, node, congestion status)	Successor nodes	Negative time	travel Tabular Q-learning	No	Using global information, i.e., congestion status in both training and execution
	This study	Multi-agent	(time, node)	Outbound links	Negative cost	travel Flow-dependent deep Q-learning	Yes	

### 1.5. Contributions of this paper

Here we will highlight the main contributions of this study as follows. First, a flow-dependent mean field deep Q-learning algorithm is developed to tackle the route choice task of multi-commodity multi-class agents. The flow-dependent mean action not only partially captures the competition among agents but also enables Q-value sharing and policy sharing. Second, we demonstrate the linkage between the classical DUE paradigm and our proposed MARL paradigm. This paper is the first-of-its-kind to unify the model-based (i.e., DUE) and data-driven (i.e., MARL) paradigms for dynamic routing games. Third, we formulate the overall task including travelers and city planners as a bilevel optimization task. We demonstrate the effect of two administrative measures, namely tolling and signal control, on the behavior of travelers and show that the systematic objective of city planners can be optimized by a proper control.

The remainder of the paper is organized as follows. Section 2 introduces the developed flow-dependent mean field multi-agent deep Q-learning algorithm. We detail the necessity and benefits of using the flow-dependent mean action which carries not full but partial information of nearby agents. Section 3 demonstrates the linkage between the classical DUE paradigm and our proposed MARL paradigm. We illustrate that actually DUE is a special case of multi-agent Markov games with a perfect information structure and a deterministic environment described by mathematical models. Section 4 introduces the bilevel optimization model where the upper level city planners can impact the behavior of lower level travelers through operational measures. A case study of the application of the bilevel optimization model to the Braess network with tolling is presented. Section 5 presents the application of the bilevel optimization model to solve for optimal traffic signal control over a real-world large-scale road network near Columbia University’s campus in the City of New York. Section 6 concludes this study.

## 2. Mean field multi-agent reinforcement learning

In this section, we introduce a flow-dependent mean field multi-agent deep Q-learning approach to tackle the multi-driver route choice task.

### 2.1. Single-agent reinforcement learning

As a stepping stone, we first introduce a single-agent RL approach. Within the single-agent scope, there is only one agent interacting with the stochastic environment. The goal of the deep Q-learning approach is to derive an optimal policy so that the agent could get the maximum expected cumulative reward by following the policy in the environment.

To be specific to the route choice task, we introduce the single-agent deep Q learning approach on a Braess network, as presented in Figure (1). In the Braess network, there are four nodes, namely  $\{n_0, n_1, n_2, n_3\}$ .  $n_0$  is the origin node and  $n_3$  the destination/terminal node. There are five directed links connecting these nodes. We denote the link connecting  $n_i$  and  $n_j$  as  $l_{ij}$ . Link travel time on  $l_{ij}$  is denoted by  $\Delta t_{ij}$ . In this study,  $\Delta t_{01} = 45$ ,  $\Delta t_{23} = 45$ ,  $\Delta t_{02} = k_{02} \cdot x$ ,  $\Delta t_{13} = k_{13} \cdot x$ , and  $\Delta t_{21} = \alpha$ , where  $x$  denotes the travel flow (i.e., number of vehicles) on the link,  $k_{02}$  and  $k_{13}$  are two multipliers, and  $\alpha$  is a control parameter.

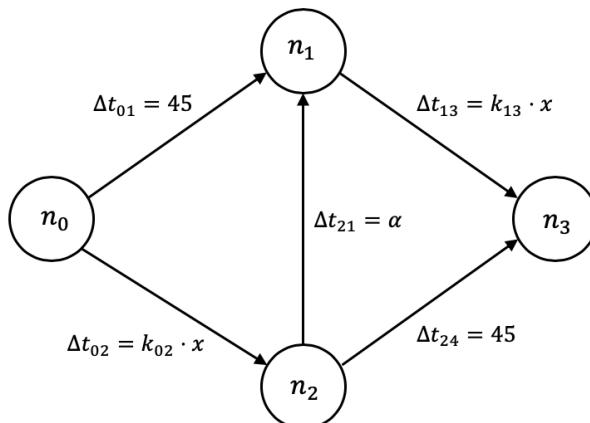


Figure 1: Braess network

First and foremost, the interaction between the agent and the environment is typically characterized by a Markov decision process or an MDP for short (Puterman, 1994). An MDP is specified by a tuple  $(S, A, R, P, \gamma)$ , where  $S$  denotes the state space,  $A$  the action space,  $R$  the reward function,  $P$  the state transition probability matrix, and  $\gamma \in [0, 1]$  the discount factor. An MDP goes as follows. At any state  $s \in S$  but some terminal state, the agent chooses action  $a \in A$  and executes the action in the environment. It observes a state transition from  $s$  to a new state  $s' \in S$  with probability  $P(s'|s, a)$  and receives a reward  $r(s, a, s') \in R$ . In the context of route choice,

- $s \in S$ . State  $s$  consists of two components, namely node and time, i.e.,  $s = (n, t)$ .
- $a \in A$ . Action  $a$  for the agent currently in state  $s = (n, t)$  is simply one of the outbound links from node  $n$ . For example,  $a = l_{n, n'}$ , where  $l_{n, n'}$  is the link connecting node  $n$  and node  $n'$ . In this study, we assume action is deterministic, meaning that the agent will enter the chosen link. Note that the number of outbound links from a node varies from node to node in the network, indicating that the number of allowable actions is dependent on the node where the agent is currently located.
- $P$ . After taking action  $a$  in state  $s$ , the agent arrives at a new state  $s' = (n', t')$  with probability  $P(s'|s, a)$ , where  $n'$  is the end node of the chosen link (i.e.,  $l_{n, n'}$ ), and  $t'$  is the time right after the state transition.  $P$  is typically unknown to the agent. Therefore, the agent needs to repeatedly interact with the environment to gain state transition experiences, i.e.,  $(s, a, s')$ .
- $r \in R$ . In addition to the observed state transition  $s \rightarrow s'$ , the agent receives a reward  $r_{t'}(s, a, s')$  after executing action  $a$ , where the subscript  $t'$  explicitly denotes that the reward is received by the agent at time  $t'$ . In the context of route choice, the reward function  $r_{t'}(s, a, s')$  is typically chosen as some negative travel cost related to the state transition  $s \rightarrow s'$ . For example,  $r_{t'}(s, a, s') = -(t' - t)$ , i.e., negative travel time, and  $r_{t'}(s, a, s') = -\text{dist}(n, n')$ , where  $\text{dist}(n, n')$  measures the distance between node  $n$  and  $n'$ , i.e., negative travel distance.
- $\gamma$ . The discount factor  $\gamma$  is used to discount the future reward. When  $\gamma = 1$ , the agent does not differentiate future rewards from immediate rewards. As  $\gamma$  get smaller, the agent cares less about rewards received in the distant future, therefore her decision-making gets more myopic. In this study, we take  $\gamma = 1$  because usually drivers aim to minimize their cumulative travel cost for a trip. In other words, they value a future travel cost and an immediate cost similarly.
- $\rho = \sum_{t=0}^T \gamma^t r_t$ .  $\rho$  is the discounted cumulative reward. The agent aims to maximize  $\rho$  by deriving an optimal policy.

The agent uses the collected experience tuples, i.e.,  $(s, a, s', r)$ , to derive an optimal policy. A policy  $\mu$  is a mapping from state  $s$  to action  $a$ , i.e.,  $\mu(s) = a$ . Following policy  $\mu$ , value function  $V^\mu(s)$  is defined as the expected discounted cumulative reward from state  $s$ . Mathematically, it is given in a recursive form, namely  $V^\mu(s) = \mathbb{E}_{a \sim \mu(s), s' \sim P(\cdot|s, a)}[r(s, a, s') + \gamma V^\mu(s')]$ . The optimal policy, denoted as  $\mu^*$ , is the policy that maximizes the value function, i.e.,  $\mu^* = \text{argmax}_\mu V^\mu(s)$ ,  $\forall s \in S$ . The optimal value function, denoted as  $V(s)$ , is given as (Sutton and Barto, 1998)

$$V(s) = \max_a \mathbb{E}_{s' \sim P(\cdot|s, a)}[r(s, a, s') + \gamma V(s')]. \quad (1)$$

While the value function  $V(s)$  captures the optimal expected cumulative reward that an agent can earn from state  $s$ , the state-action value  $Q(s, a)$  forces the agent to take action  $a$  and therefore captures the optimal expected cumulative reward from state  $s$  and action  $a$ . Mathematically,  $V(s) = \max_a Q(s, a)$ . Substituting the relation between  $V$  and  $Q$  into Equation (1) yields

$$Q(s, a) = \mathbb{E}_{s' \sim P(\cdot|s, a)}[r(s, a, s') + \gamma \max_{a'} Q(s', a')]. \quad (2)$$

With the optimal action-value function  $Q$ , optimal policy can be explicitly derived as  $\mu^*(s) = \text{argmax}_a Q(s, a)$ .

With the collected experience tuple  $(s, a, s', r)$ , the agent can update the  $Q$  value by the widely used tabular Q-learning algorithm

$$Q(s, a) \leftarrow Q(s, a) + \eta[r + \gamma \max_{a'} Q(s', a') - Q(s, a)], \quad (3)$$

where  $\eta \in (0, 1]$  is the learning rate. Convergence is guaranteed for the Q-learning algorithm when the learning rate is decayed properly over time (Sutton and Barto, 1998). Unfortunately, the tabular

Q-learning algorithm in Equation (3) is only applicable to finite and discrete state and action spaces. Tabular Q-learning maintains a Q-table for all possible combinations of state and action. It is thus not feasible to be used in a problem with large or continuous state and action spaces. Thanks to the emergence of deep Q networks (DQNs) (Mnih et al., 2015), we could resort to neural networks as a functional approximator of the Q function. Denoting the functional approximator parameterized by  $\theta$  as  $Q_\theta$ , DQN updates its parameter  $\theta$  by minimizing the following loss

$$\mathcal{L}(\theta) = \mathbb{E}_{s,a,s'} \left[ (r(s, a, s') + \gamma \max_{a'} Q_{\theta^-}(s', a') - Q_\theta(s, a))^2 \right], \quad (4)$$

where  $Q_{\theta^-}$  is called a target network copied from  $Q_\theta$  every  $\tau$  episodes to ensure training stability, where  $\tau$  is a hyperparameter.

**Example 2.1.** (Single-agent route choice).

To be more concrete, we demonstrate the aforementioned notations in the Braess network. Supposing an agent is initially placed at  $n_0$  in the Braess network, the initial state of the agent is  $s = (n_0, 0)$ . There are two allowable actions for the agent, namely  $l_{01}$  and  $l_{02}$ . Assuming the agent chooses action  $l_{02}$  in the initial state, the agent arrives at  $s' = (n_2, 1)$  with probability  $P(s' = (n_2, 1) | s = (n_0, 0), a = l_{02}) = 100\%$ . The time component in  $s'$  is 1 because the link travel time  $\Delta t_{02} = x = 1$  (i.e., there is one agent on this link). The state transition probability is 100% because both the action and the state transition are deterministic in this case. Assuming the reward function is the negative travel time, the agent receives a reward of  $-\Delta t_{02} = -1$  along with the state transition  $s \rightarrow s'$ .

We now apply the single-agent Q-learning to the Braess network with one agent initially at  $n_0$ . For the purpose of demonstration, we assume  $\alpha = 1$  and  $k_{02} = k_{13} = 40$  in this example. Due to the simplicity of this case, it could be solved analytically. Noticing the static nature of this example, we neglect the time component in state.  $n_3$  is the terminal node, meaning that  $V(n_3) = 0$ . At node  $n_1$ , the only allowable action is  $l_{13}$  leading the agent to terminal node  $n_3$ , yielding  $Q(n_1, l_{13}) = -\Delta t_{13} + \gamma V(n_3) = -40$  and  $V(n_1) = -40$ . At node  $n_2$ , there are two actions, namely  $l_{21}$  and  $l_{24}$ . Action  $l_{21}$  leads the agent to  $n_1$ , yielding  $Q(n_2, l_{21}) = -\Delta t_{21} + \gamma V(n_1) = -(\alpha + 40) = -41$ . Action  $l_{24}$  leads the agent to the terminal node  $n_3$ , yielding  $Q(n_2, l_{24}) = -\Delta t_{24} + \gamma V(n_3) = -45$ . Therefore,  $V(n_2) = \max(Q(n_2, l_{21}), Q(n_2, l_{24})) = -41$  and  $\mu^*(n_2) = l_{21}$ . At node  $n_0$ , there are two actions, namely  $l_{01}$  and  $l_{02}$ . Action  $l_{01}$  leads the agent to  $n_1$ , yielding  $Q(n_0, l_{01}) = -\Delta t_{01} + \gamma V(n_1) = -85$ . Similarly,  $Q(n_0, l_{02}) = -\Delta t_{02} + \gamma V(n_2) = -81$ . Therefore,  $V(n_0) = \max(Q(n_0, l_{01}), Q(n_0, l_{02})) = -81$  and  $\mu^*(n_0) = l_{02}$ . Following optimal policy  $\mu^*$ , the agent takes route  $n_0 \rightarrow n_2 \rightarrow n_1 \rightarrow n_3$ , which is the shortest path in this example.

## 2.2. Multi-agent reinforcement learning

Although the single-agent Q learning efficiently finds the shortest path, it fails to capture the competition among agents in a multi-agent system (MAS). In a single-agent RL problem, only one agent is placed in the environment to learn the optimal policy, which maximizes the expected cumulative reward of the agent. Unfortunately, when multiple agents follow this optimal policy, their expected cumulative reward might be low. For example, if there are 50 agents at node  $n_0$  initially in the Braess network, their expected cumulative reward is  $-110$  by following the optimal policy (i.e., the shortest path  $n_0 \rightarrow n_2 \rightarrow n_1 \rightarrow n_3$ ). This reward (i.e.,  $-110$ ) is lower than that of following another route (e.g.,  $n_0 \rightarrow n_1 \rightarrow n_3$  yields an expected cumulative reward of  $-95$ ). Therefore, to tackle a multi-driver route choice task, we develop a multi-agent deep Q-learning approach in this section to capture the competition among agents.

### 2.2.1. Problem formulation

Similar to the previous single-agent case, we introduce the multi-agent RL approach on the Braess network shown in Figure (1).

Due to the existence of multiple agents, the multi-agent RL problem is formulated as a Markov game (Littman, 1994), which is a generalization of Markov decision processes to multiple interacting agents with competing goals, in which the environment makes transitions probabilistically in response to the agents' actions. We denote the Markov game by a tuple  $(N, S, O, A, P, R, \gamma)$ , where  $N, S, O, A, P, R, \gamma$  are the number of agents, environmental state space, joint private observation space, joint action space, state transition probability functions, reward functions, and the discount factor. In the context of route choice,

- $N$ . There are  $N$  controllable adaptive agents, denoted by  $\{1, 2, \dots, N\}$ . Note that in a traffic network, there are also other traffic participants who are not controlled by the learning algorithm developed in this study. We regard those uncontrollable traffic participants as background traffic. The background traffic affects the behavior of controllable agents by its impact on link travel cost. For example, if the background traffic has caused a traffic jam on a link, it is very likely that controllable agents will avoid this jammed link.
- $\mathbf{s} \in S$ . Environmental state  $\mathbf{s}$  consists of some global information such as distribution of agents and traffic condition on each link.  $\mathbf{s}$  is not fully accessible to agents.
- $\mathbf{o} \in O$ . Although the environmental state  $\mathbf{s}$  is not observable by agent  $i$ , the agent is able to draw a private observation  $o_i \in O_i$ , which is correlated with  $\mathbf{s}$ . The Cartesian product of private observation spaces of all agents forms the joint observation space, i.e.,  $O = O_1 \times O_2 \times \dots \times O_N$ . In this paper,  $o_i$  consists of two components, namely node and time, i.e.,  $o_i = (n, t)$ . Joint observation  $\mathbf{o} = (o_1, o_2, \dots, o_N)$ .
- $\mathbf{a} \in A$ . Based on  $o_i = (n, t)$ , the allowable action set for agent  $i \in \{1, 2, \dots, N\}$  consists of all outbound links from node  $n$ . For example,  $a_i = l_{n, n'}$ , where  $l_{n, n'}$  is the link connecting  $n$  and  $n'$ . Joint action  $\mathbf{a} = (a_1, a_2, \dots, a_N)$ .
- $P$ . Joint action  $\mathbf{a}$  triggers a state transition  $\mathbf{s} \rightarrow \mathbf{s}'$  with probability  $P(\mathbf{s}'|\mathbf{s}, \mathbf{a})$ . Agent  $i \in \{1, 2, \dots, N\}$  draws a new private observations, namely  $o'_i = (n', t')$ , where  $n'$  is the end node of the chosen link  $l_{n, n'}$  and  $t'$  is the time when agent  $i$  arrives at  $n'$ . The private observation  $o'_i$  is correlated with  $\mathbf{s}'$ .
- $r \in R$ . In addition to  $o'_i$ , agent  $i \in \{1, 2, \dots, N\}$  receives a reward  $r_{i, t'}(\mathbf{s}, \mathbf{a}, \mathbf{s}')$ , where the subscript  $i, t'$  explicitly denotes that the reward is received by agent  $i$  at time  $t'$ . Similar to the single-agent RL, reward is typically some negative travel cost such as travel time and travel distance in the context of route choice.
- $\gamma$ . Similar to the single-agent RL,  $\gamma = 1$ .
- $\rho_i = \sum_{t=0}^T \gamma^t r_{i, t}$ .  $\rho_i$  is the discounted cumulative reward received by agent  $i$ . If the goal of agent  $i$  is to maximize  $\rho_i$ , agents are non-cooperative and selfish; if the goal of agent  $i$  is to maximize the average discounted cumulative rewards of all agents, i.e.,  $\frac{1}{N} \sum_{i=1}^N \rho_i$ , agents are cooperative.

Due to the coexistence of other agents,  $Q$  function of agent  $i$ , i.e.,  $Q_i$  is now a function of environmental state  $\mathbf{s}$  and joint action  $\mathbf{a}$ , namely

$$Q_i = Q_i(\mathbf{s}, \mathbf{a}). \quad (5)$$

Similarly, value function of agent  $i$ , i.e.,  $V_i$  is a function of environmental state  $\mathbf{s}$ , namely  $V_i = V_i(\mathbf{s})$ . Note that each agent  $i$  has her own  $Q$  function, i.e.,  $Q_i$ , which may be different from  $Q$  functions of other agents, and therefore has an optimal policy  $\mu_i^*$  different from policies of other agents. This distinguishes multi-agent RL from its single-agent counterpart, because agents may behave differently even in the same state with multi-agent RL while they choose the same action in the same state with single-agent RL.

Considering that environmental state  $\mathbf{s}$  is not fully observable by agents,  $Q$  function shown in Equation (5) is not tractable from the perspective of agent  $i$ . Actually, it is private observation  $o_i$  based on which agent  $i$  chooses next action. We therefore rewrite  $Q$  function for agent  $i$  as

$$Q_i = Q_i(o_i, o_{-i}, a_i, a_{-i}), \quad (6)$$

where  $o_{-i}$  and  $a_{-i}$  denote the joint observation and joint action of all agents except agent  $i$ , respectively. In a non-coordinated environment (i.e., agents are not sharing their private observations or actions),  $o_i$  and  $a_i$  are but  $o_{-i}$  and  $a_{-i}$  are not accessible to agent  $i$ . Unfortunately, removing the dependency of  $Q_i$  on  $a_{-i}$  or  $o_{-i}$  may introduce large instability in Q-learning. In addition, convergence guarantee in single-agent Q-learning is no longer valid due to the adaptive behavior of other agents if  $o_{-i}$  and  $a_{-i}$  are not included (Matignon et al., 2012).



### 2.2.2. Multi-commodity multi-class agents

For a real-world multi-agent problem, there are commonly more than tens of thousands of agents. Maintaining one  $Q$  function for each agent is thus computationally infeasible. Although heterogeneity does exist among agents (Shou et al., 2020), some agents do share some homogeneous aspects (e.g., utility function). We thus aim to reduce the number of  $Q$  functions by leveraging this homogeneity.

In the context of route choice, we focus on four aspects, namely the observation space, the action space, the reward function, and the destination. First, considering that all agents are intelligent and have the same visibility, agents share the same observation space. In other words, agents have the same observation when they arrive at the same node at the same time. Second, considering that all agents have the same freedom of choosing actions, agents share the same action space. In other words, the allowable action set is the same for agents arriving at the same node. Third, agents may have different reward functions. For example, some agents may aim to minimize their travel time while other agents may focus more on the travel distance, which is related to the fuel consumption. Therefore, agents are *multi-class*. Finally, agents may have different destinations. The reason for considering the destination as a concerned aspect is as follows. The  $Q$  function in Equation (6) essentially records the negative optimal cumulative travel cost starting from observation  $o_i$  to the destination of agent  $i$ , conditioning on action  $a_i$ , joint observation  $o_{-i}$ , and joint action  $a_{-i}$ . Therefore, agents with different destinations have different  $Q$  functions. Agents are thus said to be *multi-commodity*. In summary, we consider *multi-commodity multi-class* agents with the same observation space and the same action space in this study.

Based on the reward function and the destination of agents, we broadly categorize agents into  $C$  groups. Within each group, agents share the same state space, action space, reward function, and destination. Therefore, agents are homogeneous within each group. The multi-agent problem is then largely simplified by sharing the same  $Q$  function among agents within the same group. We denote the shared  $Q$  function for group  $c \in \{1, 2, \dots, C\}$  by

$$Q^c(o_i, o_{-i}, a_i, a_{-i}). \quad (7)$$

Note that although  $Q^c$  is shared among agents in group  $c$ , each agent has her own optimal policy  $\mu_i^*(o_i) = \operatorname{argmax}_{a_i} \mathbb{E}_{o_{-i} \sim D_{-i}, a_{-i} \sim \mu_{-i}^*} [Q^c(o_i, o_{-i}, a_i, a_{-i})]$ ,  $\forall o_i \in O_i$ , where  $D_{-i}$  denotes the distribution of  $o_{-i}$  and  $\mu_{-i}^*$  is the joint optimal policy of all agents except agent  $i$ . For example, assuming agents  $i$  and  $j$  intend to choose the same action, i.e.,  $a_i = a_j$ , at the same observation, i.e.,  $o_i = o_j$ , their expected  $Q$  values might be different, i.e.,  $\mathbb{E}_{o_{-i} \sim D_{-i}, a_{-i} \sim \mu_{-i}^*} [Q^c(o_i, o_{-i}, a_i, a_{-i})] \neq \mathbb{E}_{o_{-j} \sim D_{-j}, a_{-j} \sim \mu_{-j}^*} [Q^c(o_j, o_{-j}, a_j, a_{-j})]$ . In other words, agents have different expected  $Q$  values with respect to  $o_{-i}$  and  $a_{-i}$  even for the same observation and action pair.

### 2.2.3. Flow dependent $Q$ function

Although the number of  $Q$  functions to be maintained has been largely reduced,  $Q^c$  in Equation (7) easily becomes intractable when the number of agents in the environment gets large. Specifically, the joint observation space and the joint action space easily become prohibitively large as the number of agents increases. For example, the joint action space for 1,000 agents is  $1,000 \times d$  dimensional if each action is a  $d$  dimensional vector.

To address the above issue, we first notice that joint observation  $o_{-i}$  and joint action  $a_{-i}$  record full information of other agents, which may contain redundant information from the perspective of agent  $i$ . Actually, in the task of route choice, observations and actions of agents who are currently far away from agent  $i$  have a very limited influence on agent  $i$ . It is nearby agents who exert an impact on the traffic condition around agent  $i$ . For example, after agent  $i$  chooses a link at a node, an immediate influential quantity is the traffic flow on the chosen link. If the flow is high, agent  $i$  may experience a high travel cost on the link; if the flow is low, agent  $i$  may have a smooth transition to the end of the link. Therefore, high-dimensional  $o_{-i}$  and  $a_{-i}$  in Equation (7) could be approximated by some low-dimensional aggregate information of nearby agents. Similar to the mean field approximation in Yang et al. (2018), we call this aggregate information as the mean action of nearby agents and denote it by  $\bar{a}_i$ .  $Q$  function in Equation (7) thus becomes

$$Q^c(o_i, o_{-i}, a_i, a_{-i}) \approx Q^c(o_i, a_i, \bar{a}_i). \quad (8)$$

We now formally define the mean action in the context of route choice.

**Definition 2.1.** (*Mean action*). Mean action  $\bar{a}_i$  is defined as the traffic flow on the link that is chosen by agent  $i$ . Note that the traffic flow is calculated right after agent  $i$  enters the link.

With the above definition of the mean action, we interpret the right hand side of Equation (8), i.e.,  $Q^c(o_i, a_i, \bar{a}_i)$ , as the flow-dependent  $Q$  function.

**Definition 2.2.** (*Flow-dependent  $Q$  function*). With agent  $i$  choosing action  $a_i$  at observation  $o_i$ , the explicit inclusion of mean action  $\bar{a}_i$ , i.e., the traffic flow on the chosen link, makes  $Q^c(o_i, a_i, \bar{a}_i)$  a flow-dependent  $Q$  function.

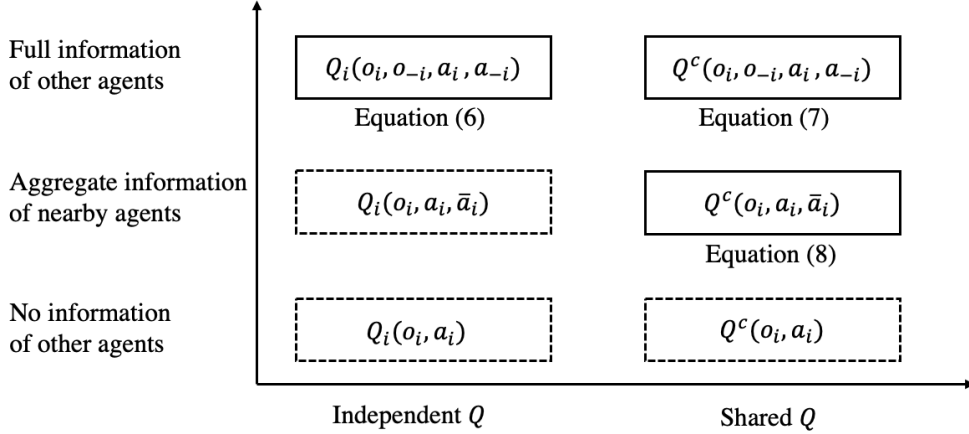


Figure 2:  $Q$  functions

We summarize the aforementioned  $Q$  functions in Figure (2). The horizontal axis indicates whether the  $Q$  function is independent (i.e.,  $Q_i$  for agent  $i$ ) or shared (i.e., homogeneous agents in group  $c$  share  $Q^c$ ). The vertical axis denotes the type of information that is used by the  $Q$  function. There are three types of information, namely full information of other agents, aggregate information of nearby agents, and no information of other agents. Consequently, there are six kinds of  $Q$  functions, as shown in Figure (2). Although  $Q$  functions in the dashed rectangle are not previously discussed, we present them in the figure for the purpose of completeness. Here we stress the advantage of the flow-dependent  $Q$  function, i.e.,  $Q^c(o_i, a_i, \bar{a}_i)$ , in an MAS with more than tens of thousands of agents. As aforementioned, independent  $Q$  functions result in maintaining tens of thousands of different  $Q$  functions and are thus computationally infeasible. Therefore, we resort to shared  $Q$  functions by considering the heterogeneity and homogeneity among agents. To be precise, now we present the advantage of the flow-dependent  $Q$  function over other two shared  $Q$  functions from two perspectives, namely a top-down perspective and a bottom-up perspective.

- The top-down perspective.  $Q^c(o_i, o_{-i}, a_i, a_{-i})$  uses full information of other agents (“top” view). Unfortunately, it is not tractable due to the prohibitively large dimension of the joint observation  $o_{-i}$  and joint action  $a_{-i}$ . Therefore, noticing the fact that the major impact on the traffic condition surrounding agent  $i$  comes from nearby agents, we approximate  $Q^c(o_i, o_{-i}, a_i, a_{-i})$  by  $Q^c(o_i, a_i, \bar{a}_i)$ .
- The bottom-up perspective.  $Q^c(o_i, a_i)$  uses no information of other agents (“bottom” view). The optimal policy for agent  $i$  in group  $c$  is  $\mu_i^*(o_i) = \operatorname{argmax}_{a_i} Q^c(o_i, a_i)$ ,  $\forall o_i \in O_i$ . Consequently, all agents in group  $c$  share the same deterministic optimal policy. This is single-agent RL instead of multi-agent RL, and we have illustrated the problem of applying single-agent RL to a multi-agent problem at the beginning of Section 2.2. To derive different policies for agents in the same group, we augment the input to the  $Q$  function by including  $\bar{a}_i$ , resulting in the flow-dependent  $Q$  function. With  $Q^c(o_i, a_i, \bar{a}_i)$ , the optimal policy for agent  $i$  in group  $c$  is  $\mu_i^*(o_i) = \operatorname{argmax}_{a_i} \mathbb{E}_{\bar{a}_i \sim \mu_{-i}^*} [Q^c(o_i, a_i, \bar{a}_i)]$ . Agent  $i$  and agent  $j$  in group  $c$  could have different policies because  $\mathbb{E}_{\bar{a}_i \sim \mu_{-i}^*} [Q^c(o_i, a_i, \bar{a}_i)]$  may be different from  $\mathbb{E}_{\bar{a}_j \sim \mu_{-j}^*} [Q^c(o_j, a_j, \bar{a}_j)]$  when  $o_i = o_j$  and  $a - i = a_j$ . In other words, agents have different expected  $Q$  values with respect to  $\bar{a}_i$  even for the same observation and action pair.

#### 2.2.4. Mean field multi-agent deep $Q$ -learning

Different from single-agent RL, agent  $i$  in group  $c \in \{1, 2, \dots, C\}$  in an MAS interacts with not only the environment but also other agents and collects experience tuples in the form of  $(o_i, a_i, o'_i, r_i, \bar{a}_i)$ .

Considering that mean action  $\bar{a}_i$  is typically in a large discrete or even continuous space, a DQN parameterized by  $\theta_c$ , denoted by  $Q^c(o_i, a_i, \bar{a}_i|\theta_c)$ , is used to approximate  $Q^c(o_i, a_i, \bar{a}_i)$ . Similar to Equation (4), DQN updates its parameter  $\theta_c$  by minimizing the following loss

$$\mathcal{L}(\theta_c) = \mathbb{E}_{o_i, a_i, \bar{a}_i, o'_i} \left[ (r_i + \gamma \max_{a'_i} \mathbb{E}_{\bar{a}'_i \sim \mu^*_{-i}} [Q^c(o'_i, a'_i, \bar{a}'_i|\theta_c^-)] - Q^c(o_i, a_i, \bar{a}_i|\theta_c))^2 \right] \quad (9)$$

where  $Q^c(\cdot|\theta_c^-)$  is a target network copied from  $Q^c(\cdot|\theta_c)$  every  $\tau$  episodes to stabilize training. After updating  $Q$  function, optimal policy

$$\mu_i^*(o_i) = \operatorname{argmax}_{a_i} \mathbb{E}_{\bar{a}_i \sim \mu^*_{-i}} [Q^c(o_i, a_i, \bar{a}_i|\theta_c)], \quad \forall o_i \in O_i. \quad (10)$$

*Remark.* Although the mean action  $\bar{a}_i$  may not be fully observable by agent  $i$ , we include it in the flow-dependent  $Q$  function, i.e.,  $Q^c(o_i, a_i, \bar{a}_i)$  during training. In execution, only the derived optimal policy  $\mu_i^*$  which is computationally a dictionary mapping from  $o_i$  to  $a_i$  is used, without involving mean action  $\bar{a}_i$ . This is essentially the idea of the centralized training and decentralized execution paradigm where some global information is used in training but not in execution (Lowe et al., 2017).

---

**Algorithm 1** Mean field multi-agent deep Q-learning (MF-MA-DQL)

---

- 1: Input: exploration parameter  $\epsilon = \epsilon_0$ , learning rate  $\eta = \eta_0$ , target network update period  $\tau$
  - 2: Initialize one DQN  $Q^c(o, a, \bar{a}|\theta)$ , parameterized by  $\theta_c$ , and one target network  $Q^c(o, a, \bar{a}|\theta_c^-)$  for each group  $c \in \{1, 2, \dots, C\}$
  - 3: Initialize  $N$  dictionaries to store the optimal policy for agents, i.e.,  $\mu_i^*, \forall i \in \{1, 2, \dots, N\}$
  - 4: Initialize one experience replay buffer  $B_c$  for each group  $c \in \{1, 2, \dots, C\}$
  - 5: Set  $episode = 0$
  - 6: **repeat**
  - 7:     From the initial environmental state  $\mathbf{s}_0$ , each agent  $i$  draws observation  $o_i$
  - 8:     Set  $t = 0$
  - 9:     **repeat**
  - 10:         For each agent  $i$ , select action  $a_i$  according to the  $\epsilon$ -greedy method, i.e., randomly select an allowable action with probability  $\epsilon$  and greedily according to policy  $\mu_i^*$  with probability  $1 - \epsilon$
  - 11:         Execute joint action  $\mathbf{a} = (a_1, a_2, \dots, a_N)$  in the environment to trigger state transition  $\mathbf{s} \rightarrow \mathbf{s}'$
  - 12:         Each agent  $i$  draws new observation  $o'_i$ , receives reward  $r_i$ , and observes mean action  $\bar{a}_i$
  - 13:         Store experience tuple  $(o_i, a_i, o'_i, r_i, \bar{a}_i)$  into replay buffer  $B_c$  if agent  $i$  belongs to group  $c$
  - 14:          $t \leftarrow t + 1$
  - 15:     **until**  $t = T$
  - 16:     **for**  $c = 1$  to  $C$  **do**
  - 17:         **for**  $j = 1$  to  $J_c$  **do**
  - 18:             Sample a batch of size  $K_c$  from replay buffer  $B_c$
  - 19:             Update parameter  $\theta_c$  of  $Q^c$  by minimizing the loss defined in Equation (9)
  - 20:             Update optimal policy  $\mu_i^*$  of agent  $i$  by Equation (10)
  - 21:         **end for**
  - 22:     **end for**
  - 23:      $episode = episode + 1$
  - 24:     Decrease the exploration parameter  $\epsilon$
  - 25:     Decrease the learning rate  $\eta$
  - 26:     **if**  $episode \bmod \tau = 0$  **then**
  - 27:         **for**  $c = 1$  to  $C$  **do**
  - 28:             Update parameter  $\theta_c^-$  of the target network, i.e.,  $\theta_c^- \leftarrow \theta_c$
  - 29:         **end for**
  - 30:     **end if**
  - 31: **until** the algorithm converges
  - 32: Return optimal policies  $\mu_i^*, \forall i \in \{1, 2, \dots, N\}$
- 

The mean field multi-agent deep Q-learning (MF-MA-DQL) algorithm is summarized in Algorithm (1). In an MAS, state transition probability functions are typically unknown due to the adaptive behavior of other agents. We therefore resort to a model-free RL approach where agents repeatedly interact with

the stochastic environment. We first initialize a centralized deep  $Q$  network, parameterized by  $\theta_c$ , and a target  $Q$  network, parameterized by  $\theta_c^-$  for each group  $c \in \{1, 2, \dots, C\}$ . Although  $Q$  function is shared among agents in the same group, each agent  $i$  in group  $c$  has her own optimal policy  $\mu_i^*$ , which is a dictionary mapping from observation  $o_i$  to action  $a_i$ . From initial environmental state  $\mathbf{s}_0$ , each agent  $i \in \{1, 2, \dots, N\}$  keeps drawing private observation  $o_i$  and taking action  $a_i$  according to the widely used  $\epsilon$ -greedy method (i.e., agent  $i$  chooses action randomly with probability  $\epsilon$  and greedily from optimal policy  $\mu_i^*$  with probability  $1 - \epsilon$ ), until reaching some terminal state. Joint action  $\mathbf{a} = (a_1, a_2, \dots, a_N)$  is executed in the environment to trigger the state transition  $\mathbf{s} \rightarrow \mathbf{s}'$ . Each agent  $i$  draws new private observation  $o'_i$ , receives reward  $r_i$ , and observes mean action  $\bar{a}_i$ . An experience replay buffer  $B_c$  for each group  $c$  is used to store experience tuple  $(o_i, a_i, r_i, \bar{a}_i, o'_i)$  generated by agent  $i$  in group  $c$ . Batch training is then used to update the centralized  $Q$  function by sampling a batch of size  $K_c$  from buffer  $B_c$  and minimizing the loss shown in Equation (9) over this batch. With the updated centralized  $Q$  function, each agent updates her optimal policy by Equation (10).

*Remark.* As a value based approach, the developed MF-MA-DQL algorithm does not suffer the problem of variable action set. A variable action set means that the number of allowable actions might vary from state to state. For example, there are two outbound links from node  $n_0$  and one outbound link from node  $n_1$  in the Braess network shown in Figure (1), causing the problem of variable action set. A policy based approach, e.g., the widely used actor-critic method, does not fit naturally well into a RL problem with variable action set. The main reason is that the policy neural network typically takes as input a state and outputs a probability distribution on all allowable actions (i.e., the action set). Consequently, a variable action set might result in some challenges to maintain a good structure of the policy network. Fortunately, value based approaches automatically handle the problem of variable action set, because a value based approach calculates the expected  $Q$  value of all possible actions at a state and selects the action with the highest  $Q$  value as the optimal policy.

**Example 2.2.** (Multi-agent route choice). Now we apply the MF-MA-DQL algorithm to a multi-agent route choice problem. In the Braess network shown in Figure (1), now two agents are initially placed at node  $n_0$ . The goal of both agents is to travel to the destination node  $n_3$  as soon as possible. Consequently, these two agents are considered to be homogeneous, because they share the same reward function (i.e., the negative travel time) and go to the same destination. We first demonstrate the notations of Markov game in this example.

There are  $N = 2$  agents in the Braess network. Environmental state  $\mathbf{s}$  is not observable, Correlated with  $\mathbf{s}$ , the joint observation of agents  $\mathbf{o} = ((n_0, 0), (n_0, 0))$ . There are two allowable actions for both agents, namely  $l_{01}$  and  $l_{02}$ . The joint action  $\mathbf{a} = (a_1, a_2)$ .  $\mathbf{a}$  triggers state transition  $\mathbf{s} \rightarrow \mathbf{s}'$  with probability  $P(\mathbf{s}'|\mathbf{s}, \mathbf{a})$ . Each agent  $i \in \{1, 2\}$  then draws new private observation  $o'_i$ , receives reward  $r_i$ , and observes mean action  $\bar{a}_i$ . To be precise, we illustrate  $o'_i$ ,  $r_i$ , and  $\bar{a}_i$  under two joint actions.

- With  $\mathbf{a} = (l_{01}, l_{02})$ ,  $o'_1 = (n_1, \Delta t_{01} = 45)$  and  $o'_2 = (n_2, \Delta t_{02} = k_{02})$ .  $r_1 = -\Delta t_{01} = -45$  and  $r_2 = -\Delta t_{02} = -k_{02}$ .  $\bar{a}_1 = 1$  and  $\bar{a}_2 = 1$ .
- With  $\mathbf{a} = (l_{02}, l_{02})$ ,  $o'_1 = (n_2, \Delta t_{02} = 2 \cdot k_{02})$  and  $o'_2 = (n_2, \Delta t_{02} = 2 \cdot k_{02})$ .  $r_1 = -\Delta t_{02} = -2 \cdot k_{02}$  and  $r_2 = -\Delta t_{02} = -2 \cdot k_{02}$ .  $\bar{a}_1 = \bar{a}_2 = 2$ .

Note that although agent 2 takes action  $l_{02}$  in both cases, the agent arrives at different observations, i.e.,  $(n_2, k_{02})$  and  $(n_2, 2 \cdot k_{02})$  due to the changing behavior of agent 1 (i.e., taking action  $l_{01}$  in the first case and  $l_{02}$  in the second).

Due to the simplicity of this case, we now analyze optimal value at each node in the network. For the purpose of demonstration, we assume  $\alpha = 10$  and  $k_{02} = k_{13} = 40$  in this example. Similar to Example 2.1, we neglect the time component in private observation due to the static nature of this problem.

1. Noticing that node  $n_3$  is the terminal node,  $V(n_3) = 0$ .
2. At node  $n_1$ , the only action that agents can take is  $l_{13}$ . After one or two agents, depending on whether both of them reach node  $n_1$ , taking action  $l_{13}$ , there are two scenarios: 1)  $\bar{a} = 1$ , i.e., traffic flow on link  $l_{13}$  is 1, meaning currently there is only one agent on link  $l_{13}$  and it takes the agent  $\Delta t_{13} = k_{13} \cdot 1 = 40$  to reach node  $n_3$ , therefore  $Q(o = n_1, a = l_{13}, \bar{a} = 1) = -40$ ; 2)  $\bar{a} = 2$ , i.e., traffic flow on link  $l_{13}$  is 2, meaning that there are two agents on link  $l_{13}$  and it takes the agent  $\Delta t_{13} = k_{13} \cdot 2 = 80$  to reach node  $n_3$ , therefore  $Q(o = n_1, a = l_{13}, \bar{a} = 2) = -80$ . Note that in scenario 2), it could be either both agents choose action  $l_{13}$  at node  $n_1$  simultaneously or one

agent chooses action  $l_{13}$  first because she arrives at  $n_1$  first and the other agent chooses action  $l_{13}$  later due to her later arrival at node  $n_1$  (e.g., one agent chooses route  $n_0 \rightarrow n_1$  and arrives at  $n_1$  at  $t = 45$ , and the other agent chooses route  $n_0 \rightarrow n_2 \rightarrow n_1$  and arrives at  $n_1$  at  $t = k_{02} + \alpha = 50$ ). In the former case, both agents observe  $\bar{a} = 2$  and spend time 80 on their way to  $n_3$ ; in the latter case, the agent who arrives at  $n_1$  first observes  $\bar{a} = 1$  and spends time 40 on her way to  $n_3$  and the other agent observes  $\bar{a} = 2$  and spends time 80. With  $Q(n_1, l_{13}, 1) = -40$  and  $Q(n_1, l_{13}, 2) = -80$ , optimal value at  $n_1$ , i.e.,  $V(n_1)$ , is within the range of  $[-40, -80]$  and depends on the distribution of  $\bar{a}$ .

3. At node  $n_2$ , there are two outbound links, namely  $l_{21}$  and  $l_{23}$ . If one or two agents at  $n_2$  choose action  $l_{21}$ ,  $Q(n_2, l_{21}, \bar{a}) = -\alpha + \gamma \times V(n_1) = -10 + V(n_1)$ , which is lower than  $-50$ , regardless of  $\bar{a}$ . If one or two agents at  $n_2$  choose action  $l_{23}$ ,  $Q(n_2, l_{23}, \bar{a}) = -\Delta t_{23} = -45$ . Therefore, action  $l_{21}$  is strictly dominated by action  $l_{23}$ , indicating that optimal policy at  $n_2$  for both agents is to choose action  $l_{23}$  and  $V(n_2) = -45$ .
4. Finally, at node  $n_0$ , there are two possible actions, namely  $l_{01}$  and  $l_{02}$ , and both agents choose action simultaneously. There are 3 possible scenarios: 1) when both agents choose action  $l_{01}$ ,  $Q(n_0, l_{01}, \bar{a} = 2) = -\Delta t_{01} + \gamma V(n_1) = -45 + (-80) = -125$ . Note that  $V(n_1) = -80$  because both agents arrive at node  $n_1$  and choose action  $l_{13}$  at the same time. 2) when both agents choose action  $l_{02}$ ,  $Q(n_0, l_{02}, \bar{a} = 2) = -\Delta t_{02} + \gamma V(n_2) = -80 + (-45) = -125$ . 3) when one agent chooses action  $l_{01}$  and the other chooses action  $l_{02}$ ,  $Q(n_0, l_{01}, \bar{a} = 1) = -\Delta t_{01} + \gamma V(n_1) = -45 + (-40) = -85$  and  $Q(n_0, l_{02}, \bar{a} = 1) = -\Delta t_{02} + \gamma V(n_2) = -40 + (-45) = -85$ . Note that  $V(n_1) = -40$  because only one agent uses link  $l_{13}$ . Therefore, the optimal policy of one agent is to choose action  $l_{01}$  and that of the other agent is to choose action  $l_{02}$  at  $n_0$ .

In summary, optimal values of interest are listed in Table 2. Link  $l_{21}$  is not used by agents because it is strictly dominated by  $l_{23}$ . From  $n_0$ , the payoff for agents are  $(-85, -85)$  if they choose actions differently and  $(-125, -125)$  if they choose the same action (i.e., either  $l_{01}$  or  $l_{02}$ ). Therefore, optimal policy of one agent is to choose action  $l_{01}$  and that of the other is to choose  $l_{02}$ , and this is a Nash equilibrium because no agent can get better payoff by a unilateral deviation.

Table 2: Optimal values of interest

observation $o$	action $a$	mean action $\bar{a}$	$Q(o, a, \bar{a})$	$V(o)$
$n_1$	$l_{13}$	1	-40	$V(n_1) = \mathbb{E}_{\bar{a}}[Q(n_1, l_{13}, \bar{a})]$ is within the range of $[-80, -40]$ .
$n_1$	$l_{13}$	2	-80	
$n_2$	$l_{21}$	1 or 2	$\leq -50$	Action $l_{23}$ strictly dominates $l_{21}$ . $V(n_2) = Q(n_2, l_{23}, \bar{a}) = -45$ .
$n_2$	$l_{23}$	1 or 2	-45	
$n_0$	$l_{01}$	1	-85	$V(n_0) = -85$ if agents choose actions differently at $n_0$ and $V(n_0) = -125$ if agents choose the same action.
$n_0$	$l_{01}$	2	-125	
$n_0$	$l_{02}$	1	-85	
$n_0$	$l_{02}$	2	-125	

### 3. Linkage between DTA and Markov games

Dynamic traffic assignment has been widely used to model route choice behavior of travelers. A general DTA problem typically consists of two parts, namely a dynamic network loading (DNL) module and a route choice model.

**DNL.** Given traffic demand and route choices, the DNL module propagates traffic flow dynamics and/or traffic congestion through the network. There are two components in the DNL module, namely a link model and a junction model. A link model is used to propagate inflow traffic demand to exit and is usually described by either a delay/latency function or an exit-flow function (Nie and Zhang, 2005). As for the former, both linear delay functions and nonlinear functions (e.g., the widely used BPR function) are used in the literature. As for the latter, there are a large body of literature proposing or using various exit-flow functions such as the M-N model (Merchant and Nemhauser, 1978a,b), the point-queue model (Kuwahara and Akamatsu, 1997; Ban et al., 2012a), and the cell transmission model (Daganzo, 1994, 1995). A junction model is used to determine the flow distribution at an intersection.

**Route choice.** Route choice models guide travelers to properly choose next go-to links right before they arrive at a node/intersection. According to the objective of travelers, there are typically two types of research problems, namely dynamic system optimum (DSO) and dynamic user equilibrium (DUE). While DSO aims to minimize total or average travel cost of all travelers (Ziliaskopoulos, 2000), DUE describes the equilibrium state in which no individual traveler could decrease her travel cost by unilaterally deviating from her current route choices (Friesz and Han, 2019; Friesz et al., 2013).

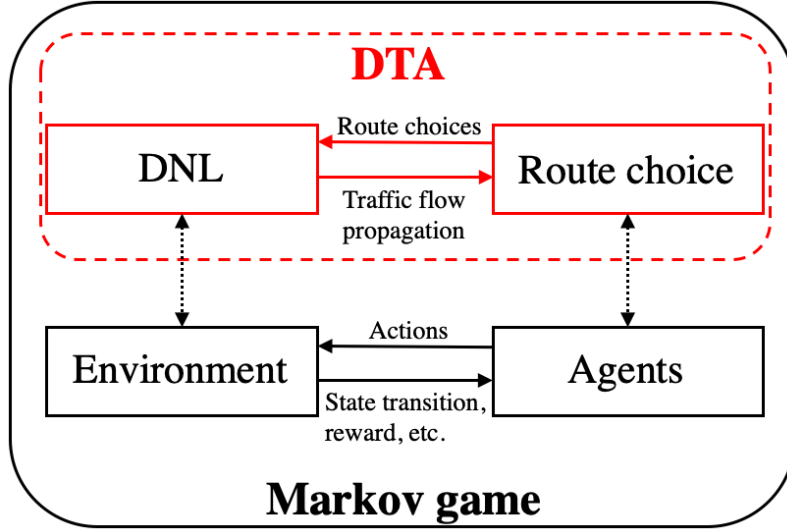


Figure 3: Connection between DTA and Markov game

With the aforementioned Markov game and DTA, we now discuss the connection between DTA and the corresponding Markov game (i.e., in the context of route choice). Recall that there are two components in a DTA, namely a DNL module and a route choice model, and two components in a Markov game, namely an environment and agents. The connection between DTA and Markov game is componentwise, as schematically presented in Figure (3). The DNL in DTA is regarded as the environment in Markov game, and the route choices in DTA are made by agents in Markov game. Further, the interaction between the DNL and route choice in DTA is similar to that between the environment and agents in Markov game. In DTA, a route choice model outputs route choices of travelers whenever they arrive at a node or an intersection, and the DNL module propagates traffic flow dynamics. In Markov game, agents (i.e., travelers) take actions (i.e., route choices) whenever they arrive at a node, and the environment experiences a state transition which is determined by the DNL module in DTA. To be precise, the actions taken by agents in Markov game are route choices in DTA, and the state transition, rewards, etc. in Markov game are determined by the DNL module in DTA.

In summary, DUE is essentially a special case of multi-agent Markov games with a perfect information structure and a deterministic environment described by mathematical models. Compared to generic Markov games, the DTA paradigm might suffer from several shortcomings:

1. Computational efficiency of algorithms of solving a dynamic user equilibrium (DUE) might be highly compromised in large-sized road networks.
2. Stochasticity arising from traffic environments is challenging to model in the DTA paradigm. Such randomness comes from various sources, including demand side (such as random numbers of travelers) and supply side (such as weather, accidents, or events). The existing DTA approaches typically require an explicit functional form of the stochastic sources (Peeta and Zhou, 1999; Waller and Ziliaskopoulos, 2001; Sumalee et al., 2011). In addition, adaptive route choice behavior of other agents may contribute to the inherent stochasticity in traffic evolution, which has not been generally accounted for in the existing DTA paradigm.
3. A majority of DUE models cannot depict the adaptive behavior of travelers along a route, in other words, individuals' next-go-to link choice at a node based on cumulative travel costs to destinations. This is because either path-based choice representation is adopted that disables en-route choice at

intermediate nodes (Friesz et al., 2013; Friesz and Han, 2019), or because future traffic conditions along a route are not accounted for even when next-go-to link selection is modeled (Ban et al., 2012b). Although we acknowledge that some specially design DUE methods might be able to capture en-route adaptive behavior of drivers, it could be hard to solve.

4. Rather than modeling individual agents' route choice behavior, DUE models are non-atomic games focused on aggregate traffic flow evolution, which renders them not flexible to accommodate heterogeneity in travelers. Such aggregation could also render these models fail to accommodate individual observations such as travel trajectories or mobile traces.
5. A fundamental issue in prescriptive models is their inability to adapt to real-time observations. In other words, its calibration and validation process is open-loop even when presented with real-world data (such as vehicle trajectories or aggregate flows). For instance, the common practice is to calibrate parameters of a DTA model offline and then run the calibrated model for prediction. The calibration and prediction processes are thus separated. With the emergence of sensing and communication technologies, an explosive amount of vehicle driving trajectories and mobile traces can be obtained, which warrants adaptive models in which agents are capable of learning prevailing traffic environment while adjusting their en-route path choice dynamically.

Given these shortcomings, we will demonstrate how Markov games can solve dynamic routing games with imperfect information structure and a stochastic model-free environment. Before delving into it, we will first illustrate on numerical examples the equivalence between DUE or DSO and the equilibria computed from our developed MARL algorithm.

### 3.1. Numerical example

We first apply the developed MF-MA-DQL algorithm to a two-node two-link network, as presented in Figure (4a). Two nodes are denoted by  $O$  (origin) and  $D$  (destination), respectively. There are two links, namely link 0 with length  $l_0 = 20$  and link 1 with length  $l_1 = 10$ . Further, we take free flow speed on link 0 as 5, i.e.,  $v_0 = 5$  and that on link 1 as 2, i.e.,  $v_1 = 2$ . In other words, during light traffic, it takes a vehicle  $l_0/v_0 = 4$  time steps to travel from node  $O$  to node  $D$  via link 0 and  $l_1/v_1 = 5$  time steps via link 1. We denote the time-varying travel demand from node  $O$  to node  $D$  by  $d(t)$ .

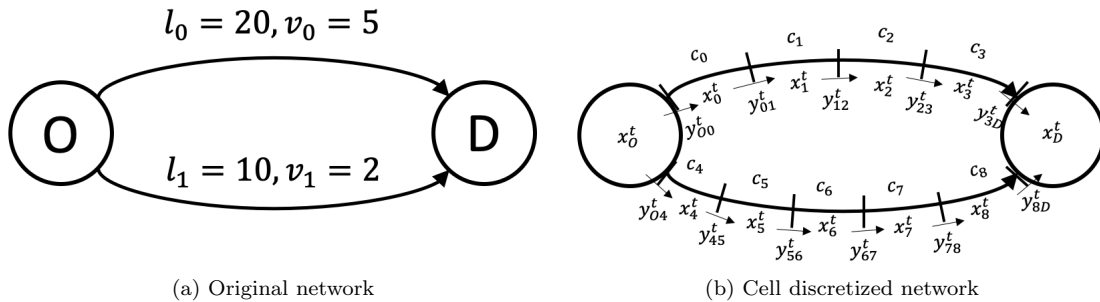


Figure 4: A two-node two-link network

After vehicle drivers making route choices, the traffic propagation (i.e., dynamic network loading) is described by the widely used cell transmission model (CTM) (Daganzo, 1994, 1995). The first thing in a CTM is to discretize each link into several cells. The length of each cell is supposed to be the distance traveled by a vehicle in light traffic. Therefore, in the two-node two-link network, the length of a cell on a link is essentially the free flow velocity on this link. Consequently, there are four cells of length 5 on link 0 and five cells of length 2 on link 1, respectively. The resulting cell discretization is presented in Figure (4b). Each cell is denoted by  $c_i$ , where  $i \in \{0, 1, \dots, 8\}$ .  $x_i^t$  records the number of vehicles in cell  $i$  at time  $t$ , and  $y_{ij}^t$  is the flow from cell  $i$  to cell  $j$  at time  $t$ . Noticing that the demand goes from node  $O$  to node  $D$ , there are  $x_O^t$  and  $x_D^t$  recording the number of vehicles on nodes and  $y_{O0}^t$ ,  $y_{O4}^t$ ,  $y_{3D}^t$ , and  $y_{8D}^t$  denoting the flow from and to nodes. For notation simplicity, we denote the upstream cells of cell  $i$  as  $\Gamma^{-1}(i)$  and downstream cells of cell  $i$  as  $\Gamma(i)$ . According to the flow conservation, the number of vehicles

in cell  $i \in \{0, 1, \dots, 8\}$  at time  $t + 1$  equals to the number of vehicles in the cell at time  $t$  plus the inflow and minus the outflow, namely

$$x_i^{t+1} = x_i^t + \sum_{k \in \Gamma^{-1}(i)} y_{ki}^t - \sum_{j \in \Gamma(i)} y_{ij}^t. \quad (11)$$

While Equation (11) applies to the destination node  $D$ , the time-dependent demand term, i.e.,  $d(t + 1)$  needs to be added to the right hand side of the equation for the origin node  $O$ . The flow between cells on either link is governed by the following equation

$$y_{ij}^t = \min(x_i^t, Q_{ij}^t, N_j^t - x_j^t), \quad (12)$$

where  $Q_{ij}^t$  is the maximum allowed flow rate between cells  $i$  and  $j$  at time  $t$ , and  $N_j^t$  denotes the capacity of cell  $j$  at time  $t$ . Equation (12) indicates that the flow between two cells is restricted by (1) the number of vehicles in the upstream cell (i.e.,  $x_i^t$ ), (2) the maximum flow rate between these two cells, and (3) the remaining capacity of the downstream cell. As suggested in Daganzo (1994), Equation (12) implicitly assumes that the density wave backward propagation speed is equal to the free flow speed. Otherwise, there is supposed to be a coefficient  $\delta$ , which is the ratio of the free flow speed to the wave backward propagation speed, in front of the remaining capacity of the downstream cell. In this case study, we follow the explanations in Daganzo (1994) and assume that the density wave propagates backwards at the speed of free flow. Similarly, for the flow into or out of nodes, we have the following inequality conditions

$$\begin{aligned} y_{O0}^t + y_{O4}^t &\leq x_O^t, \quad y_{O0}^t \leq Q_{O0}^t, \quad y_{O0}^t \leq N_0^t - x_0^t, \quad y_{O4}^t \leq Q_{O4}^t, \quad y_{O4}^t \leq N_4^t - x_4^t, \\ y_{3D}^t + y_{8D}^t &\leq N_D^t - x_D^t, \quad y_{3D}^t \leq Q_{3D}^t, \quad y_{3D}^t \leq x_3^t, \quad y_{8D}^t \leq Q_{8D}^t, \quad y_{8D}^t \leq x_8^t. \end{aligned}$$

With the aforementioned CTM propagating traffic, now we apply the developed MF-MA-DQL algorithm to two scenarios, namely a fully cooperative scenario where all selfless vehicles aim to minimize the average travel cost of all vehicles and a competitive scenario where each selfish vehicle aims to minimize her own travel cost. The optimal route choice from the former yields a dynamic system optimum (DSO), and that from the latter yields a dynamic user equilibrium (DUE). Due to the simplicity of the two-node two-link network, we employ an analytical solution, i.e., a linear programming formulation (Ziliaskopoulos, 2000), for the DSO scenario and a numerical solution, i.e., an iterative method (Gawron, 1998), for the DUE scenario as baselines. We then compare the result from the MF-MA-DQL method to that from the corresponding baseline in both scenarios.

To complete the setup, without loss of generality, we use the discretized two-node two-link network presented in Figure (4b) with cell capacities  $N_i = 4, \forall i \in \{0, 1, 3, 4, 5, 6, 8\}$  and  $N_i = 2, \forall i \in \{2, 7\}$ , maximum allowed flow rate between cells  $Q_{ij} = 2, \forall ij \in \{01, 12, 23, 45, 56, 67, 78\}$ , and maximum flow rate between cell and node  $Q_{O0} = Q_{O4} = Q_{3D} = Q_{8D} = 4$ . In addition, the time-dependent demand is given as

$$d(t) = \begin{cases} 20, & t = 0 \\ 40, & t = 5 \\ 10, & t = 10. \end{cases}$$

### 3.1.1.1. Dynamic system optimum (DSO)

To achieve a DSO, all vehicles using the network behave cooperatively and aim to minimize their average travel cost, or equivalently their total travel cost.

#### 3.1.1.1.1 MF-MA-DQL for DSO

As aforementioned, the local observation of agent  $i$  contains two components, namely a node component  $n$  and a time component  $t$ . Recall that vehicles only make route choices when they are at a node. In the two-node two-link network, agents only choose their actions at the origin node  $O$ , indicating that the node component could be removed from the local observation. Therefore,  $o_i = t$  in this case study. When agents are at node  $O$ , there are two allowable actions, namely either link 0 or link 1. Therefore, the action space for agent  $i$  is  $a_i \in \{\text{link 0}, \text{link 1}\}$ . After agent  $i$  executing action  $a_i$  with observation  $o_i$ , the agent observes a mean action  $\bar{a}_i$ , i.e., the number of agents on the link chosen by agent  $i$ , and travels



to the destination node  $D$  following the traffic propagated by the CTM. To achieve DSO, the reward for agent  $i$  is defined as the negative average travel time of all agents, mathematically,

$$r_i = -\frac{1}{N} \sum_{i=1}^N \Delta t_i^{OD},$$

where  $\Delta t_i^{OD}$  stands for the travel time from node  $O$  to node  $D$  of agent  $i$ . In other words, in the DSO scenario, all agents receive the same amount of reward after executing their actions. With such definition of reward function, agents behave cooperatively to minimize the average travel time and achieve DSO.

### 3.1.1.2 A linear programming formulation

Noticing that there is exactly one destination node in the two-node two-link network, we employ the linear programming (LP) approach developed in Ziliaskopoulos (2000) and Liu et al. (2007) to solve the single-destination DSO problem. Mathematically, the LP formulation is

$$\text{Minimize } \sum_{t=0}^T (x_O^t + \sum_{i=0}^8 x_i^t). \quad (13)$$

subject to

$$x_i^{t+1} = x_i^t + \sum_{k \in \Gamma^{-1}(i)} y_{ki}^t - \sum_{j \in \Gamma(i)} y_{ij}^t, \forall i \in \{0, 1, \dots, 8, D\}, \quad (14)$$

$$x_i^{t+1} = x_i^t - \sum_{j \in \Gamma(i)} y_{ij}^t + d(t+1), \text{ when } i = O, \quad (15)$$

$$y_{ij}^t = \min(x_i^t, Q_{ij}^t, N_j^t - x_j^t), \forall i \in \{0, 1, \dots, 8\}, \quad (16)$$

$$y_{O0}^t + y_{O4}^t \leq x_O^t, \quad y_{O0}^t \leq Q_{O0}^t, \quad y_{O0}^t \leq N_0^t - x_0^t, \quad y_{O4}^t \leq Q_{O4}^t, \quad y_{O4}^t \leq N_4^t - x_4^t, \quad (17)$$

$$y_{3D}^t + y_{8D}^t \leq N_D^t - x_D^t, \quad y_{3D}^t \leq Q_{3D}^t, \quad y_{3D}^t \leq x_3^t, \quad y_{8D}^t \leq Q_{8D}^t, \quad y_{8D}^t \leq x_8^t, \quad (18)$$

$$x_i^0 = 0, \forall i \in \{0, 1, \dots, 8, D\}, \quad x_O^0 = d(0), \quad (19)$$

where the objective is to minimize the total travel cost of all vehicles. Equations (14) and (15) are the flow conservation, Equations (16), (17), and (18) state the restrictions on the flow between cells, Equation (19) is the initial condition.

### 3.1.1.3 Comparison between the LP solution and MF-MA-DQL solution

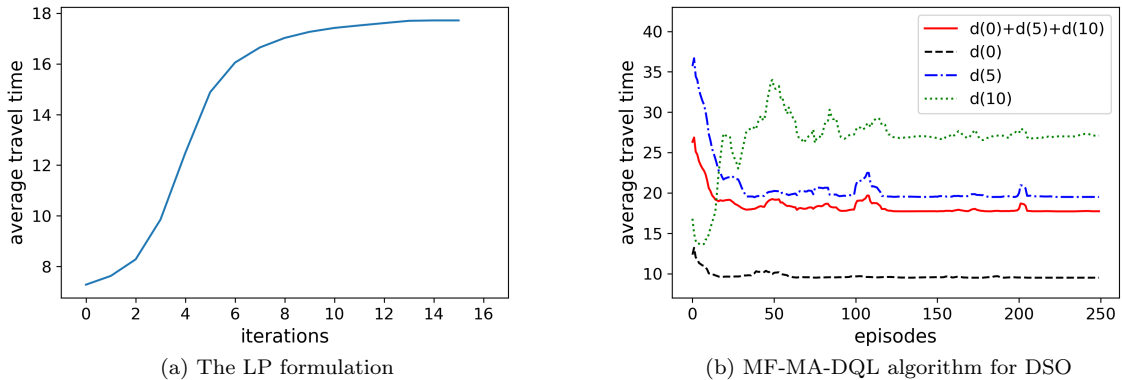


Figure 5: Convergence plots for DSO

Convergence plots of both methods for the DSO scenario are presented in Figure (5). For the LP formulation, it takes 15 iterations to reach convergence, as shown in Figure (5a). The converged value

of the average travel time of all vehicles is 17.7. For the MF-MA-DQL algorithm, after bouncing back and forth during the first 150 episodes in Figure (5b), the average travel time of all vehicles (i.e.,  $d(0) + d(5) + d(10)$ ) gradually reaches its converged value at 17.7, which agrees well with its analytical counterpart from the LP formulation. In addition, the converged average travel times of  $d(0)$ ,  $d(5)$ , and  $d(10)$  are 9.5, 19.5, and 26.9, respectively. It is worthwhile to mention that the average travel time of  $d(0)$  converges faster than that of  $d(5)$  and  $d(10)$ . This is as expected because the later demand has no effect on the earlier demand, under the assumption that overtaking does not occur. In other words, it takes some extra time for the average travel time of the later demand to achieve convergence, after that of the earlier demand has reached convergence. As for the optimal policy, 10 vehicles from  $d(0)$ , 21 vehicles from  $d(5)$ , and 5 vehicles from  $d(10)$  choose link 0, and the remaining vehicles choose link 1.

### 3.1.2. Dynamic user equilibrium (DUE)

For a DUE problem, Wardrop’s first principle, i.e., travel cost on all used routes for any given origin-destination pair is supposed to be the same, is a widely accepted guideline to derive DUE solutions. In other words, at equilibrium, no individual selfish vehicle could decrease her travel cost by unilaterally deviating from her current route choice strategy.

#### 3.1.2.1 MF-MA-DQL for DUE

All MF-MA-DQL settings such as the definition of local observation and action remain the same as those in MF-MA-DQL for DSO, except for the definition of the reward function. Recall that in DSO, the reward for an cooperative agent is the negative average travel time of all agents using the network. While in DUE, the reward for a non-cooperative agent is simply the negative of her own travel cost. In other words, instead of aiming to minimize the average travel cost of all cooperative agents in DSO, each non-cooperative agent aims to minimize her own travel cost in DUE.

#### 3.1.2.2 An iterative method

Noticing that the simple form of the objective in Equation (13) is no longer applicable to DUE problems, we employ the iterative method proposed in Gawron (1998). The basic idea of the iterative method is to let vehicles choose routes according to some policy and then calculate the network loading and travel cost by simulation so that vehicles gradually learn towards better route choices. By iterating this process, a stationary fixed point solution is supposed to be derived so that no vehicle could get better off by switching her route choices. To make this paper self-explanatory, we now briefly introduce the iterative method adapted to the two-node two-link network. Interested readers could refer to Gawron (1998) for more details.

---

#### Algorithm 2 An iterative method to solve DUE

---

- 1: Initialize a proportion  $p_t(0)$  indicating the proportion of the demand at  $t$  choosing link 0. Consequently,  $p_t(1) = 1 - p_t(0)$
  - 2: Initialize a learning step size  $\eta \in (0, 1]$
  - 3: Initialize function  $g(x) = \exp(\frac{ax}{1-x^2})$ , where  $a$  is a parameter, and function  $f(x) = \frac{p_t(0)g(x)}{p_t(0)g(x) + p_t(1)}$
  - 4: **repeat**
  - 5:     Calculate the time-dependent travel cost of both links, denoted by  $\tau_t(0)$  and  $\tau_t(1)$ , from simulation
  - 6:     Calculate the relative cost difference  $\delta_{01} = \frac{\tau_t(1) - \tau_t(0)}{\tau_t(1) + \tau_t(0)}$
  - 7:     Update the proportion by  $p_t(0) = (1 - \eta)p_t(0) + \eta f(\delta_{01})$
  - 8:     Calculate  $p_t(1) = 1 - p_t(0)$
  - 9:     Update function  $f(x) = \frac{p_t(0)g(x)}{p_t(0)g(x) + p_t(1)}$
  - 10: **until** the iterative method reaches a stationary fixed point
  - 11: Return  $p_t(0)$  and  $p_t(1)$
- 

The iterative method is listed in Algorithm (2). With demand  $d(t)$  emerging from node  $O$  at time  $t$ , we randomly initialize  $p_t(0)$  and  $p_t(1)$  to denote the proportion of the demand choosing link 0 and link 1, respectively. We also initialize functions  $g(x)$  and  $f(x)$  which will be used to update  $p_t(0)$  and

$p_t(1)$ . Note that  $f : [-1, 1] \rightarrow [0, 1]$  is a monotonic increasing function. With  $p_t(0)$  and  $p_t(1)$ , we run simulation to calculate the average travel cost on both links for the demand starting at time  $t$  and denote these time-dependent travel cost by  $\tau_t(0)$  and  $\tau_t(1)$ . We then calculate the relative cost difference  $\delta_{01} = \frac{\tau_t(1) - \tau_t(0)}{\tau_t(1) + \tau_t(0)}$  and use this cost difference to update the proportion  $p_t(0)$  towards  $f(\delta_{01})$  by step size  $\eta$ . The rationale of this updating rule is as follows. When  $\delta_{01}$  is large (e.g., close to 1), meaning that the cost on link 0 is much less than that on link 1, we have  $f(\delta_{01}) \approx 1$ , indicating that  $p_t(0)$  is updated towards a larger value; when  $\delta_{01}$  is small (e.g., close to  $-1$ ), meaning that the cost on link 0 is much larger than that on link 1, we have  $f(\delta_{01}) \approx 0$ , indicating that  $p_t(0)$  is updated towards a smaller value. After updating  $p_t(0)$  and  $p_t(1)$ , we repeat the iterative process until reaching a stationary fixed point.

### 3.1.2.3 Comparison between the solution of the iterative method and MF-MA-DQL solution

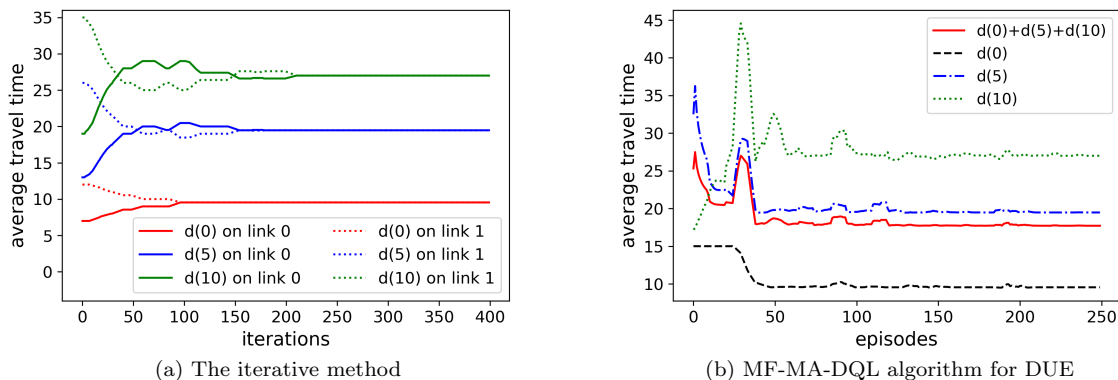


Figure 6: Convergence plots for DUE

Convergence plots of both methods for the DUE scenario are presented in Figure (6). In Figure (6a), the average travel time for each batch of demand (i.e.,  $d(0)$ ,  $d(5)$ , and  $d(10)$ ) on each link (i.e., link 0 and link 1) is plotted. For example, for  $d(0)$ , there is a certain proportion of  $d(0)$  choosing link 0 (we call this part  $d(0)$  on link 0) and the remaining proportion choosing link 1 (we call this part  $d(0)$  on link 1). Initially,  $d(0)$  on link 1 experiences a higher average travel time than  $d(0)$  on link 0. The iterative method then updates  $p_0(0)$  (i.e., the proportion of  $d(0)$  choosing link 0) to be larger and  $p_1(0)$  to be smaller. The average travel time will thus become larger on link 0 and lower on link 1. Recall that the iterative method reaches convergence when the average travel times on both links become the same. After 220 iterations, the average travel times on both links for all batches of demand converge. The converged average travel times for  $d(0)$ ,  $d(5)$ , and  $d(10)$  are 9.6, 19.5, and 27.0, respectively.

For the MF-MA-DQL algorithm, after bouncing back and forth during the first 120 episodes in Figure (6b), average travel times of  $d(0)$ ,  $d(5)$ ,  $d(10)$ , and  $d(0) + d(5) + d(10)$  gradually reach their converged values 9.6, 19.6, 27.0, and 17.7, respectively, which agree well with the values derived from the iterative method. As for the optimal policy, 11 vehicles from  $d(0)$ , 19 vehicles from  $d(5)$ , and 6 vehicles from  $d(10)$  choose link 0, and remaining vehicles choose link 1.

### 3.1.3. DSO versus DUE

The agreement between the LP solution and the MF-MA-DQL solution in the DSO scenario and that between the solution from the iterative method and MF-MA-DQL solution in the DUE scenario validate the effectiveness of the developed MF-MA-DQL algorithm. Here we stress that the MF-MA-DQL algorithm is more versatile and could be applied to cooperative, competitive, and even mixed scenarios.

It is worth mentioning the difference between DSO and DUE in this two-node two-link network. Table (3) listed the average travel time and optimal policy for each batch of demand in both DSO and DUE scenarios. Although one could see that both the average travel time and the optimal policy seem quite similar for these two scenarios, DSO and DUE are intrinsically different. For the purpose of demonstration, we analyze the first batch of demand, i.e.,  $d(0)$ . In the DSO scenario, the optimal policy

suggests 10 vehicles to choose link 0 and the other 10 vehicles to choose link 1. The average travel time for the 10 vehicles on link 0 is 9 and that for the remaining 10 vehicles on link 1 is 10, indicating that average travel times on two used links could be different in the DSO scenario. The average travel time of these 20 vehicles is 9.5. In the DUE scenario, the optimal policy suggests 11 vehicles to choose link 0 and the other 9 vehicles to choose link 1. The average travel time for both the 11 vehicles on link 0 and the remaining 9 vehicles on link 1 is 9.6. The average travel time of these 20 vehicles is 9.6. In summary, the average travel time is lower in the DSO scenario where the average travel times on used links could be different; while in the DUE scenario, the Wardrop first principle is respected.

Table 3: DSO versus DUE

	average travel time				optimal policy (choosing link 0)		
	$d(0)$	$d(5)$	$d(10)$	$d(0) + d(5) + d(10)$	$d(0)$	$d(5)$	$d(10)$
DSO	9.5	19.5	26.9	17.7	10	21	5
DUE	9.6	19.5	27.0	17.7	11	19	6

#### 4. Bilevel optimization for multi-agent route choice

Traffic congestion has become one of the major issues faced by modern cities. With the limited transportation network capacity, traffic congestion occurs when there are too many vehicles using the road network, especially on some critical links. To mitigate traffic congestion, in addition to increasing the infrastructure supply which could be costly, city planners can actually resort to tolling to redistribute traffic demand on the network and improve the overall traffic condition. While imposing a toll charge on a critical link may make the link less attractive to travelers, similar to the effect of decreasing the capacity of the link, no toll may attract too many travelers to the link and result in traffic congestion or even jam on this link, as the Braess paradox suggests (Steinberg and Zangwill, 1983; Pas and Principio, 1997). In other words, compared with no tolling, a proper toll on a critical link could redistribute some traffic to other links and consequently improve the overall traffic condition.

In this section, we aim to investigate the effect of tolling a critical link on the overall traffic network. Note that from the perspective of travelers, the overall travel cost is the summation of their travel time and the toll charge paid out of their pocket. Without loss of generality, we assume that the travel time and toll charge could directly be added without unit conversion. In other words, we assume travelers value their time and monetary cost similarly. We study the effect of tolling a link on the Braess network, as presented in Figure (1). There are some travelers from origin node  $n_0$  to terminal node  $n_3$ , and the travel time on link  $l_{21}$ , i.e.,  $\Delta t_{21} = \alpha$ . We regard  $\alpha$  as the toll charge on link  $l_{21}$ . A larger  $\alpha$  means that the toll is higher, indicating that there might be fewer travelers choosing the link; while a smaller  $\alpha$  means that the toll is lower, indicating that more travelers may choose this link. We aim to find an optimal value of  $\alpha$  with which some overall systematic performance such as the average travel time of all vehicle drivers is optimized. We denote this systematic performance by  $f$ .

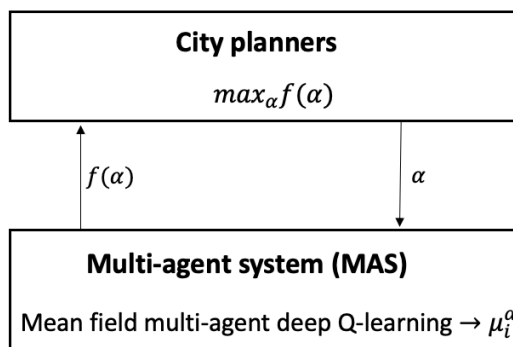


Figure 7: Bilevel optimization model

As aforementioned, behavior of travelers change with the adjustment in  $\alpha$ . In this study, we assume that drivers are perfectly rational and leave bounded rationality (Di et al., 2013) in future research. Recall

that our goal is to find the optimal  $\alpha$ , therefore we formulate this as a bilevel optimization problem, as presented in Figure (7). The upper level is city planners aiming to maximize the systematic performance  $f$  and has some control, parameterized by  $\alpha$ , over the lower level MAS. In the lower level MAS, each agent  $i \in \{1, 2, \dots, N\}$  derives her optimal policy  $\mu_i^\alpha$  by the developed MF-MA-DQL algorithm presented in the previous section. Note that we use superscript  $\alpha$  in the notation of optimal policy, i.e.,  $\mu_i^\alpha$ , to signify the dependency of optimal policy on the control parameter  $\alpha$ . With optimal behavior of all agents, city planners observe the systematic performance  $f(\alpha)$ . City planners then adjust control parameter  $\alpha$  until reaching optimum.

Due to the unknown complex structure of  $f$  over  $\alpha$ , traditional gradient based methods are not applicable. In addition, evaluation of  $f$  at one value of  $\alpha$  using MARL is computational expensive. Therefore, we resort to Bayesian optimization (BO) which does not require gradient and is especially efficient at optimizing some objectives that is expensive to evaluate (Frazier, 2018). The procedure of BO is as follows. First, BO places a statistical model on the objective function  $f$ , such as a Gaussian process. Second, BO devises an acquisition function such as upper confidence bound (UCB) (Srinivas et al., 2010) to decide where to evaluate next, i.e., to choose an  $\alpha$  based on the statistical model. Third, BO updates the statistical model based on the newly evaluated  $\alpha$ , and the process repeats. The pseudo-code of BO is listed in Algorithm (3). Interested readers are referred to (Frazier, 2018) for more details on BO.

---

**Algorithm 3** Bayesian Optimization

---

- 1: Initialize a Gaussian process prior on  $f$
  - 2: Evaluate  $f$  at  $n_0$  different  $\alpha$ s according to certain rules
  - 3: Set computational budget  $N$  and  $n = n_0$
  - 4: **while**  $n \leq N$  **do**
  - 5:     Update posterior probability distribution on  $f$  based on all evaluated  $\alpha$ s
  - 6:     Calculate an acquisition function
  - 7:     Locate the  $\alpha_n$  which maximizes the acquisition function
  - 8:     Evaluate  $f$  at  $\alpha_n$
  - 9:      $n \leftarrow n + 1$
  - 10: **end while**
  - 11: Return  $\alpha_n$  which maximizes  $f$
- 

#### 4.1. Numerical example

We now apply the bilevel optimization model to the Braess network presented in Figure (1). The rationale of adopting the Braess network in this section is as follows. First, the Braess network is simple, and usually an analytical solution could be derived, meaning that we could compare our numerical solution to its analytical counterpart. Second, recall that our goal is to find an optimal  $\alpha$  with which the overall systematic performance (i.e., average travel time of all drivers in the Braess network) is optimized. The existence of Braess paradox in the Braess network makes our goal nontrivial.

##### 4.1.1. Lower level: validation of the MF-MA-DQL on Braess network

We first validate the developed MF-MA-DQL algorithm in two cases, namely a case with single-batch demand and a case with multi-batch demand. Details of the setup of each case will be discussed later. In both cases, we initialize a multilayer perceptron (MLP) with three hidden layers (32, 16, 8) to approximate the centralized  $Q$  function. ReLU is the activation function used between hidden layers. Learning rate  $\eta = 10^{-3}$ . Exploration parameter  $\epsilon$  is initially set as 0.1, i.e.,  $\epsilon_0 = 0.1$ , and linearly decreases to 0.01. The target network update period  $\tau = 5$ , meaning that target network  $Q(o, a, \bar{a}|\theta^-)$  is copied from the principal network, i.e.,  $Q(o, a, \bar{a}|\theta)$  every 5 episodes.

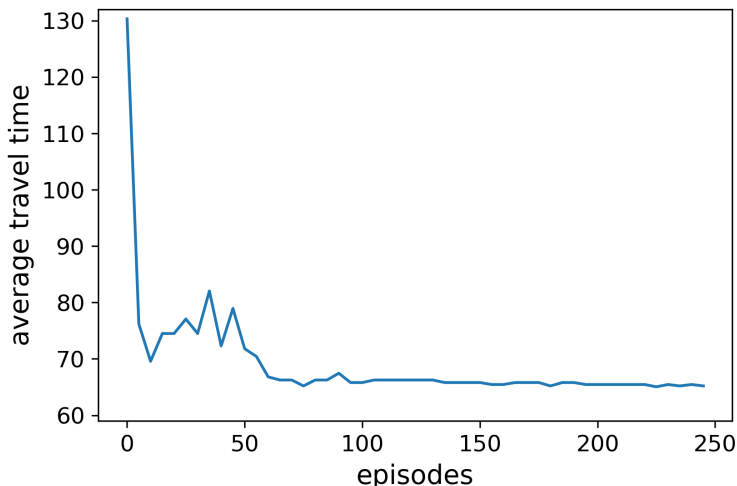


Figure 8: Convergence of MF-MA-DQL algorithm in the case with single-batch demand

In the case with single-batch demand, number of drivers initially at origin node  $n_0$  is set as 40, and  $k_{02} = k_{13} = 1$ . We further assume  $\alpha = 100$ , i.e., a very large number, indicating that link  $l_{21}$  is not supposed to be used by any agent after training in this case. The convergence of the MF-MA-DQL algorithm for this case is presented in Figure (8). The y axis is the average travel time of all 40 agents from origin node  $n_0$  to terminal node  $n_3$ . The x axis shows the number of episodes. Initially, because agents are moving around randomly to explore the environment, the average travel time is as high as 130. During the first 10 episodes, the average travel time decreases very fast to around 70, indicating agents are learning towards a better policy. After some bouncing back and forth, the average travel time reaches its converged value at 65 after 100 episodes. The derived optimal policy shows that 20 agents choose route  $n_0 \rightarrow n_1 \rightarrow n_3$  and the other 20 choose route  $n_0 \rightarrow n_2 \rightarrow n_3$ .

The analytical solution for this case could be derived as follows. First, notice that route  $n_0 \rightarrow n_1$  strictly dominates route  $n_0 \rightarrow n_2 \rightarrow n_1$ , because  $\Delta t_{02} + \Delta t_{21} > \Delta t_{01}$  always holds. Similarly, route  $n_2 \rightarrow n_3$  strictly dominates route  $n_2 \rightarrow n_1 \rightarrow n_3$ . Therefore, rational agents will not use  $l_{21}$  under any circumstances. Consequently, there are only two reasonable routes from  $n_0$  to  $n_3$ , namely  $n_0 \rightarrow n_1 \rightarrow n_3$  and  $n_0 \rightarrow n_2 \rightarrow n_3$ . Assuming there are  $y$  agents choosing the former and  $40 - y$  agents choosing the latter, at equilibrium, if both routes are used, the travel time on both routes is supposed to be the same. Otherwise, some agents currently on the route with a larger travel time could deviate and choose the other route to decrease their travel time. Mathematically,

$$45 + k_{13} \cdot y = k_{02} \cdot (40 - y) + 45,$$

where the left hand side is travel time on the former route and the right hand side is travel time on the latter route. By some simple linear algebra,

$$y = \frac{40 \cdot k_{02}}{k_{02} + k_{13}}. \quad (20)$$

Plugging  $k_{02} = k_{13} = 1$ ,  $y = 20$ , meaning that at equilibrium, 20 agents choose the former route and 20 choose the latter. Travel time for all agents at equilibrium is 65. Both travel time and optimal policy from previous numerical solution agree well with their analytical counterparts from the analytical solution. Here we stress that this case validates the effectiveness of the developed MF-MA-DQL algorithm. Although all agents share one centralized  $Q$  function, agents find different optimal policies. In comparison, if a single-agent deep Q-learning was adopted to tackle this multi-agent problem, agents share a centralized  $Q$  function and one optimal policy. Unfortunately, a shared optimal policy guides all agents to use the same route, which is definitely not optimal for agents. For example, the travel time for an agent would be  $45 + 40 = 85$  if all 40 agents choose either route  $n_0 \rightarrow n_1 \rightarrow n_3$  or route  $n_0 \rightarrow n_2 \rightarrow n_3$ .

Actually, the aforementioned case is symmetric, because travel time on both routes is  $45 + x$ , where  $x$  is the flow (i.e., number of agents) choosing the route. To further test the effectiveness of the MF-MA-DQL

algorithm in asymmetric cases, we break the symmetry by keeping  $k_{02} = 1$  and varying  $k_{13}$ . Specifically, we test the MF-MA-DQL algorithm with 10 different values of  $k_{13}$ , namely  $k_{13} \in \{1, 2, \dots, 10\}$ . Other parameters such as  $\alpha$  and number of agents remain unchanged. With respect to the analytical solution, it follows Equation (20) with  $k_{02} = 1$ , yielding  $y = \frac{40}{1+k_{13}}$  and travel time for all agents as  $45 + \frac{40 \cdot k_{13}}{1+k_{13}}$ , at equilibrium. Note that the analytical solution applies to both integer and fractional  $k_{13}$ . The comparison of average travel time between the numerical solution (i.e., using MF-MA-DQL) and analytical solution is presented in Figure (9). The y axis is the average travel time of all agents after convergence under a given  $k_{13}$ . All red dots (i.e., numerical solution) are on the blue curve (i.e., analytical solution), indicating a very good agreement between the numerical and analytical solution. This validates the effectiveness of the developed MF-MA-DQL algorithm in asymmetric cases.

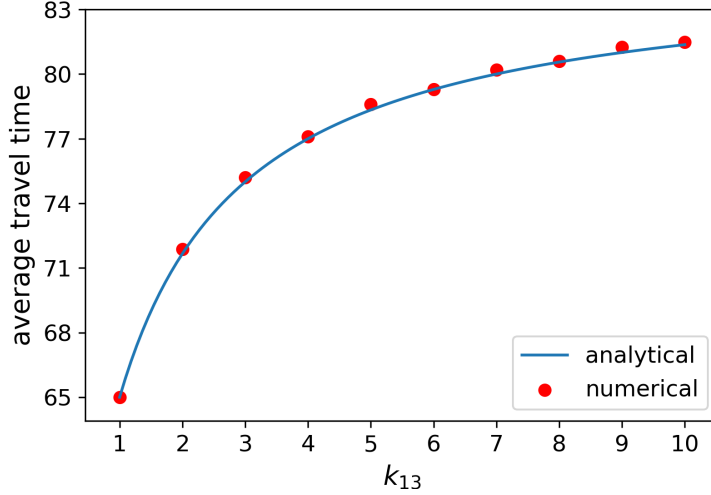


Figure 9: Comparison between numerical solution and analytical solution with varying  $k_{13}$

After validating the MF-MA-DQL algorithm in the case with single-batch demand, we now aim to further validate it in a case with multi-batch demand. Similar to the case with single-batch demand, number of drivers initially at origin node  $n_0$  is set as 40. In addition, another 20 drivers will depart from  $n_0$  at time  $t = 10$ . For notation simplicity, we call 40 agents who depart from  $n_0$  at  $t = 0$  the first 40 agents and 20 agents who depart from  $n_0$  the latter 20 agents. In this case, route choice of the first 40 agents has impact on behavior of the latter 20 agents, because the first 40 agents are on some links and thus travel time on those links could be larger. We further assume  $\alpha = 1$  in this case.

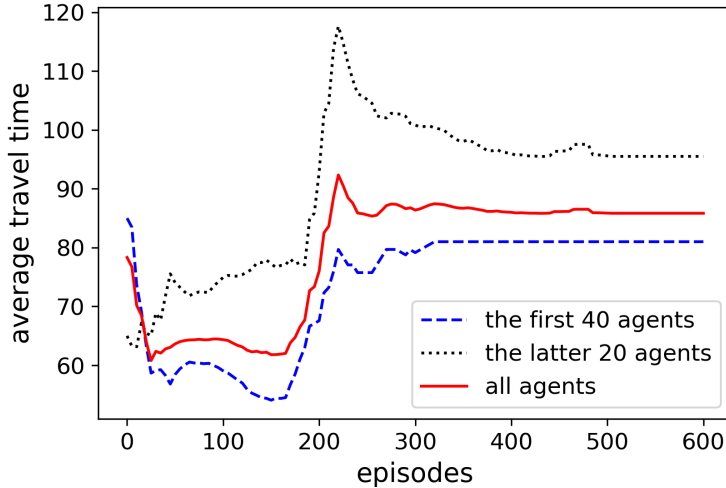


Figure 10: Convergence of MF-MA-DQL algorithm in the case with multi-batch demand

Figure (10) presents the average travel time of the first 40 agents, the latter 20 agents, and all 60 agents, respectively, versus the number of training episodes. The first 40 agents explore the environment and learn towards their optimal policies during the first 300 episodes. It is noteworthy that the average travel time of the first 40 agents decreases fast, then bounces back and forth below 60, and finally increases fast to around 80. The reason is as follows. Initially the first 40 agents act according to the randomly initialized centralized  $Q$  function and there is no experience accumulated, indicating that agents choose the same route (e.g.,  $n_0 \rightarrow n_1 \rightarrow n_3$ ), resulting in a large travel time of 85. After some exploration, some agents learn that the average travel time of other routes are lower (e.g.,  $n_0 \rightarrow n_2 \rightarrow n_1 \rightarrow n_3$ ). Therefore, these agents are now choosing the route with a lower travel time, leading to a lower average travel time (e.g., below 60). As more and more agents learn this better route with lower travel time, the average travel time increases, because the traffic flow (i.e., number of agents) on this route increases. The average travel time of the first 40 agents reaches its converged value at 81 after 300 episodes, and the optimal policy is to choose route  $n_0 \rightarrow n_2 \rightarrow n_1 \rightarrow n_3$ . Actually, with  $\alpha = 1$ , route  $n_0 \rightarrow n_2 \rightarrow n_1$  strictly dominates route  $n_0 \rightarrow n_2$ , because  $\Delta t_{02} > \Delta t_{01} + \Delta t_{12}$  always holds. Similarly, route  $n_2 \rightarrow n_1 \rightarrow n_3$  strictly dominates route  $n_2 \rightarrow n_3$ . Therefore, the analytical optimal policy for the first 40 agents is to choose route  $n_0 \rightarrow n_2 \rightarrow n_1 \rightarrow n_3$  with average travel time  $\Delta t_{02} + \Delta t_{21} + \Delta t_{13} = 40 + 1 + 40 = 81$ . As for the latter 20 agents, their average travel time and optimal policies are strongly affected by the first 40 agents. Actually, after the average travel time of the first 40 agents converges at 300 episodes, it takes another 100 episodes for the average travel time of the latter 20 agents to converge. It is as expected because behavior of the first 40 agents has impact on that of the latter 20 agents, while the behavior of 20 agents has no effect on that of the first 40 agents, under the assumption that overtaking does not occur. In other words, after the first 40 agents find their optimal policy, the latter 20 agents need to keep exploring the environment to derive their own optimal policy. After 400 episodes, the average travel time of the latter 20 agents reaches its converged value at 95, which is consistent with the value from analytical solution. Note that due to similarity, we omit the derivation of analytical solution here.

#### 4.1.2. Bilevel: emergence of Braess paradox and the optimal toll pricing

After validating the MF-MA-DQL algorithm in aforementioned cases, we now run bilevel optimization on the Braess network with  $k_{02} = k_{13} = 1$  and  $\alpha$  as the control variable of upper level city planners. Similar to case with single-batch demand, initially there are 40 travelers at node  $n_0$ . In other words, with the demand as 40 agents from  $n_0$  to  $n_3$ , we aim to find the optimal  $\alpha$  with which the average travel time of these 40 agents could be optimized. To be precise, the negative average travel time of these 40 agents is taken as the objective  $f$  of the upper level city planners. The range of  $\alpha$  is set as  $[0, 45]$ . A case with  $\alpha > 45$  is trivial because  $\Delta t_{02} + \Delta t_{21} > \Delta t_{01}$  and  $\Delta t_{21} + \Delta t_{13} > \Delta t_{23}$  always hold. Therefore,  $n_0 \rightarrow n_1$  dominates  $n_0 \rightarrow n_2 \rightarrow n_1$  and  $n_2 \rightarrow n_3$  dominates  $n_2 \rightarrow n_1 \rightarrow n_3$ , indicating that link  $l_{21}$  will not be taken by any agent.



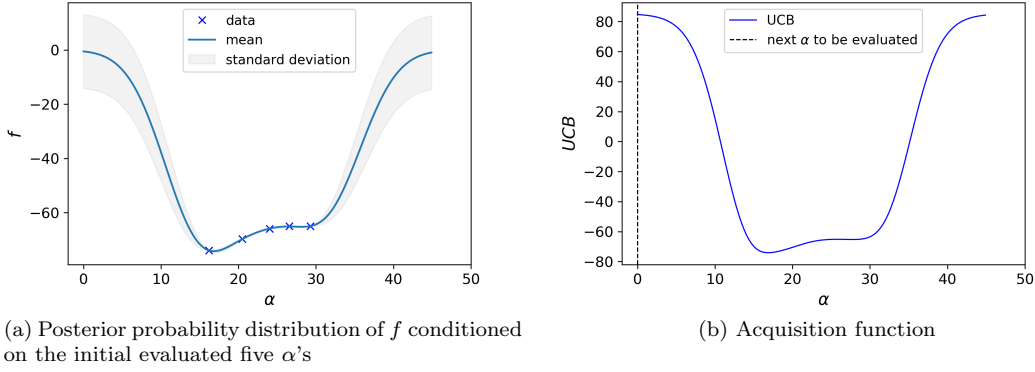


Figure 11: Posterior probability distribution and acquisition function at iteration 0

With the problem well defined, we use BO to solve the bilevel problem. As for the starting point of BO, we evaluate objective  $f$  at five randomly sampled  $\alpha$ 's. Figure (11a) presents the posterior probability distribution of  $f$  conditioned on these five initially evaluated  $\alpha$ 's. As one can see, standard deviation is small near evaluated  $\alpha$ 's while large around locations with no evaluated data. Acquisition function used in this study is UCB and is plotted in Figure (11b). Based on the acquisition function, the next  $\alpha$  to be evaluated is 0.

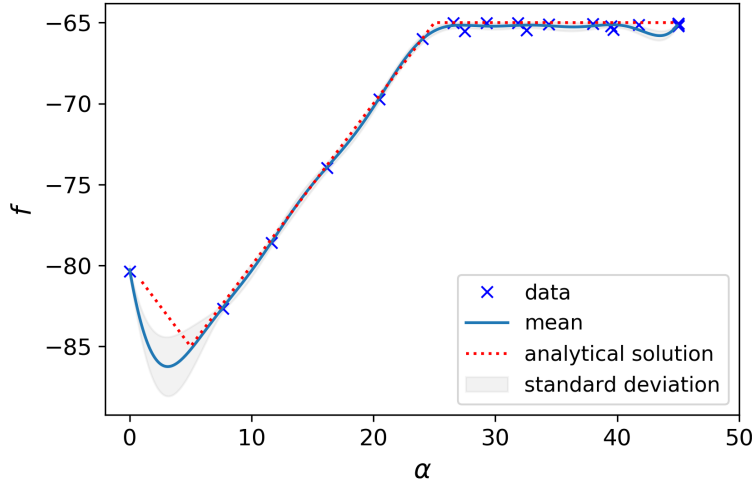


Figure 12: Posterior probability distribution of  $f$

We then run BO for 15 iterations. In other words, we assume there is some computational budget of 15 evaluations of  $f$ . The posterior probability distribution of  $f$  along with the analytical solution is plotted in Figure (12). The derivation of analytical solution is detailed as follows. From node  $n_0$  to node  $n_3$ , there are in total three possible routes, namely route  $n_0 \rightarrow n_1 \rightarrow n_3$ , route  $n_0 \rightarrow n_2 \rightarrow n_1 \rightarrow n_3$ , and route  $n_0 \rightarrow n_2 \rightarrow n_3$ . Assuming there are  $y_1$  agents choosing the first route,  $y_2$  agents choosing the second route, and  $40 - y_1 - y_2$  choosing the last route, at equilibrium, travel time on these routes is supposed to be the same, if all of them are used. Therefore, we have the following equation

$$45 + y_1 + y_2 = y_2 + (40 - y_1 - y_2) + (y_1 - 1 + y_2) = y_2 + (40 - y_1 - y_2) + 45.$$

By some simple linear algebra, we solve for  $y_1$  and  $y_2$  as follows

$$\begin{aligned} y_1 &= \alpha - 5, \\ y_2 &= 50 - 2\alpha. \end{aligned}$$

In addition, there are constraints on number of agents choosing a route, i.e.,  $0 \leq y_1 \leq 40$  and  $0 \leq y_2 \leq 40$ . These constraints yield  $5 \leq \alpha \leq 25$ . Actually, with  $\alpha < 5$ , it can be easily seen that only route  $n_0 \rightarrow n_2 \rightarrow n_1 \rightarrow n_3$  is used by agents; while with  $\alpha > 25$ , route  $n_0 \rightarrow n_2 \rightarrow n_1 \rightarrow n_3$  is not used by any agent. Therefore, the objective  $f$ , i.e., negative average travel time, versus  $\alpha$  could be solved as

$$f(\alpha) = \begin{cases} -(80 + \alpha), & \alpha < 5 \\ -(90 - \alpha), & 5 \leq \alpha \leq 25 \\ -65, & \alpha > 25. \end{cases}$$

The analytical is plotted as the red dotted line in Figure (12). The overall good agreement between the analytical solution and numerical solution validates the bilevel optimization model.

With  $\alpha = 0$  (i.e., no toll), the optimal route choice, from both the numerical and analytical solution, for all agents is to use route  $n_0 \rightarrow n_1 \rightarrow n_2 \rightarrow n_3$ , and the average travel time of all agents is 80; with  $\alpha > 25$  (i.e., a large toll), the optimal route choice is half of agents using route  $n_0 \rightarrow n_1 \rightarrow n_3$  and the other half using route  $n_0 \rightarrow n_2 \rightarrow n_3$ , and the average travel time of all agents is 65. This indicates that a small toll (i.e., a shorter travel time) on link  $l_{12}$  actually increases the overall travel time of all agents, resulting in the emergence of Braess paradox. In other words, decreasing the travel cost on a link by either expanding the capacity of the link or reducing the toll charge on the link may not benefit the overall traffic condition. On the contrary, it (i.e., decreasing the travel cost on a link) may deteriorate the overall traffic condition by attracting too many travelers to the link. In this case study, the optimal toll pricing on link  $l_{12}$  is a travel time greater than or equal to 25, which yields the optimal systematic objective.

## 5. Case Study

In this section, we apply the developed bilevel optimization model to a real-world road network with 69 nodes and 166 links, as presented in Figure (13). This road network covers the area from 135th Street (south) to 145th Street (north) and from Riverside Drive (west) to Convent Avenue (east) in upper Manhattan. In addition to Riverside Drive and Convent Avenue, there are Broadway and Amsterdam Avenue in the north-south direction. The road network is imported into SUMO.

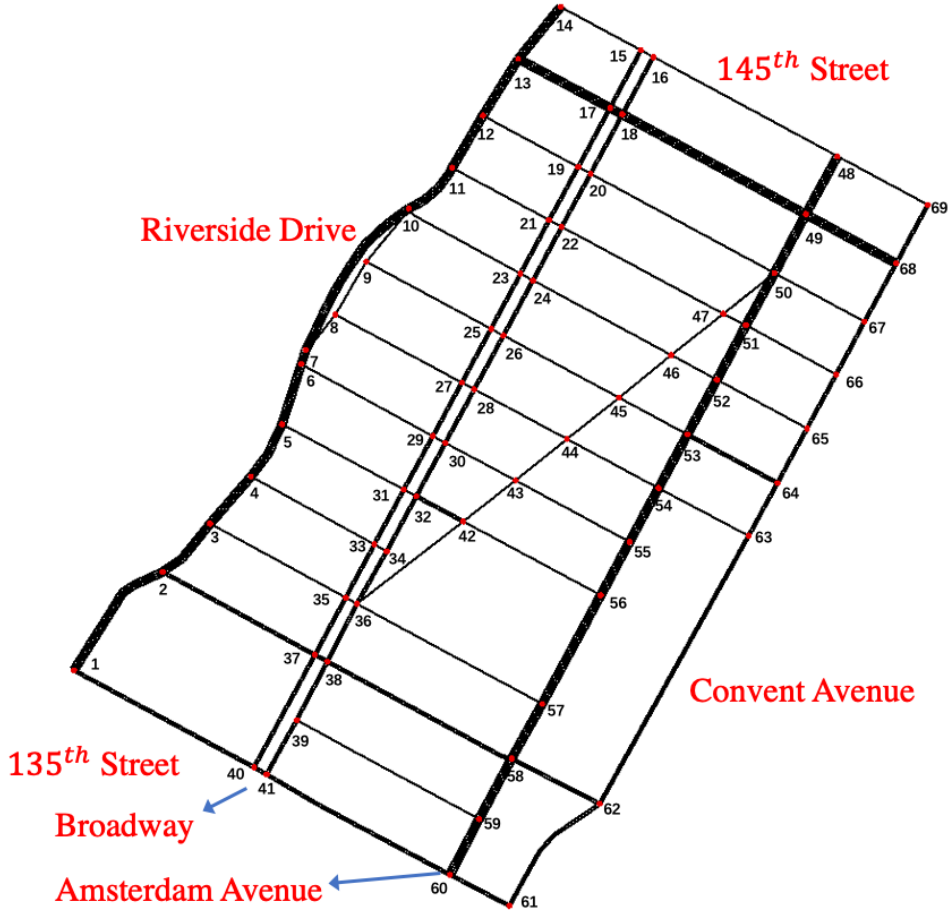


Figure 13: Road network in SUMO

### 5.1. Setup of the bilevel problem

Now we detail the setup of the bilevel problem.

#### 5.1.1. Lower level: controllable agents and background traffic

There are two types of vehicles in the road network, namely controllable agents and background traffic. The former actively adapts her route choices while the latter constantly follows some prescribed travel pattern. In this case study, there are four groups of controllable agents: 1) three agents travel from node 14 to node 60, 2) three agents from node 15 to node 60, 3) three agents from node 48 to node 1, and 4) three agents from node 69 to node 1. With respect to the background traffic, there are in total around 1,600 vehicles in the south-north direction and 500 vehicles in the east-west direction within the simulation time period (i.e., 1000 seconds).

The goal of each controllable agent is to minimize her travel cost from origin to destination. Noticing that the first two groups of controllable agents share the same destination, i.e., node 60, these agents thus share the same  $Q$  function. We denote this  $Q$  function as  $Q^{60}$ , where the superscript 60 indicates that this  $Q$  function is used by agents whose destination is node 60. Obviously,  $Q$  value at destination node is 0, i.e.,  $Q^{60}(o_i = (60, t), a_i, \bar{a}_i) = 0$ , regardless of time  $t$ , action  $a_i$ , and mean action  $\bar{a}_i$ . Similarly, the remaining controllable agents whose destination is node 1 share the same  $Q$  function, which is denoted by  $Q^1$ .  $Q^1(o_j = (1, t), a_j, \bar{a}_j) = 0$ .

#### 5.1.2. Upper level: signal control

With the controllable agents aiming to minimize their travel time and background traffic following a prescribed traffic profile, city planners can affect the route choice behavior of adaptive controllable agents by adjusting the traffic signals at intersections, i.e., signal control. The goal of city planners is to develop a proper signal control scheme so that the average travel time of all controllable agents is minimized.

In this study, we assume that city planners only adjust traffic signals on Broadway. In addition, we assume that there are green light with fixed duration of 60 seconds and red light with fixed duration of 30 seconds on Broadway. The only controllable variable is the offset between green lights of two consecutive intersections on Broadway. To be precise, we formally define the offset below.

**Definition 5.1.** (*Offset* (Hu and Liu, 2013)). The offset between green lights of two consecutive intersections is the difference between starting time of green light at one intersection and that at the previous upstream intersection.

For example, along the north-south direction, the difference between the starting time of green light at node 17 and that at node 15 is the offset. Note that in this study, we assume that the same offset applies to every two consecutive intersections on Broadway. For example, the offset of node 17 and node 15 is the same as that of node 19 and node 17.

Denoting the negative average travel time of all controllable agents as  $f$  and the offset as  $\alpha$ , we have  $f(\alpha)$ , meaning that  $f$  is dependent on  $\alpha$ . The rationale underlying such dependency is partially explained as follows. With different values of  $\alpha$  (i.e., the offset), controllable agents may experience different travel times. For example, with a proper  $\alpha$ , controllable agents may take advantage of “green wave” on Broadway and thus spend less time reaching their destination, leading to a larger  $f$ . On the contrary, with a poorly chosen  $\alpha$ , controllable agents may need to stop frequently and spend more time on waiting at the intersection, resulting in a smaller  $f$ . The goal is to find the optimal  $\alpha^*$  which maximizes  $f$ , i.e.,

$$\alpha^* = \operatorname{argmax} f(\alpha).$$

## 5.2. Results

With the aforementioned setup, we run the bilevel optimization model until convergence.

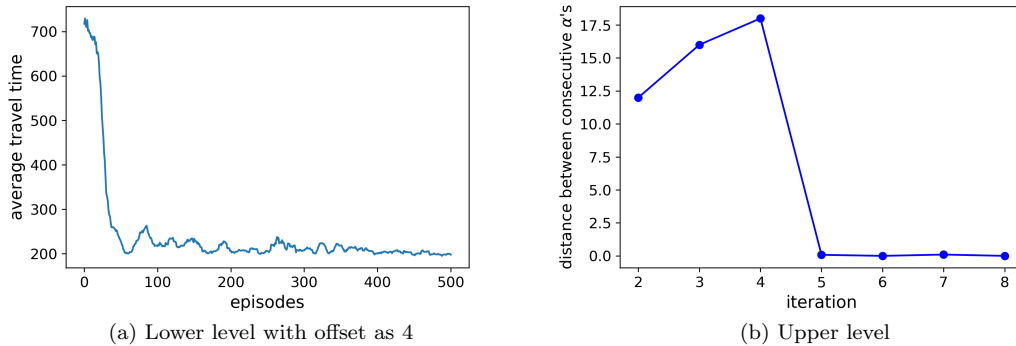


Figure 14: Convergence of BO

Convergence plots of both the lower level flow-dependent deep Q-learning and the upper level BO are presented in Figure (14). Figure (14a) presents the variation of the average travel time of all controllable agents versus the number of episodes. Initially, agents spend a very long time (i.e., more than 700 seconds) on traveling to their destinations. Actually, some agents may not be able to reach their destinations and could record a total travel time of 1,000 seconds (i.e., the maximum allowed time in one episode). During the first 60 episodes, agents explore the road network and learn towards a better policy pretty fast. Therefore, their average travel time is substantially decreased from above 700 seconds to around 200 seconds. Despite some bouncing back and forth between 60 episodes and 300 episodes, the average travel time of all controllable agents stabilizes around 200 seconds after 300 episodes. Especially after 400 episodes, the average travel time almost barely changes. Figure (14b) presents the distance between two consecutive evaluated  $\alpha$ 's in the BO algorithm. A smaller distance means that BO chooses to evaluate similar  $\alpha$ 's, indicating that the algorithm approaches convergence. In this study, we stop the BO algorithm when the distance is smaller than a threshold value (i.e., 2.5) for four times in a row. With five randomly selected  $\alpha$ 's as starting point, BO reaches convergence after 9 additional iterations. As one could see, BO selects very different  $\alpha$ 's during the first 4 iterations and starts selecting similar  $\alpha$ 's from the 5<sup>th</sup> iteration.

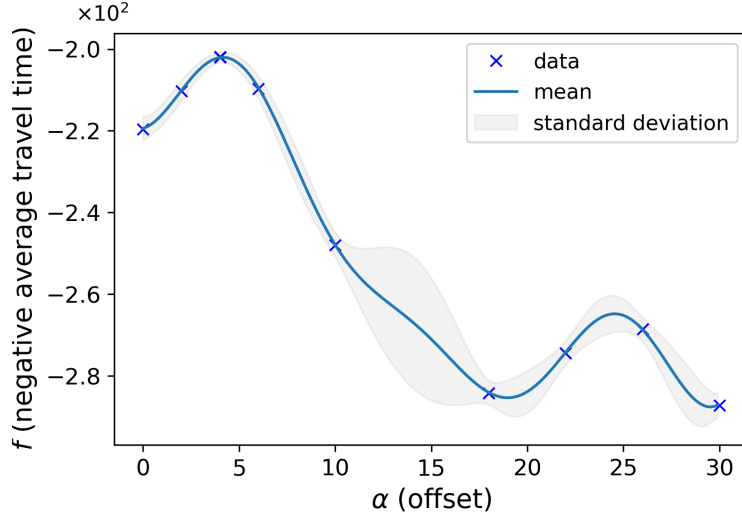


Figure 15: Posterior probability distribution of  $f$  at the 8<sup>th</sup> iteration

With the illustrated convergence of both levels, the final result of the posterior probability distribution of the objective  $f$  (i.e., the negative average travel time) is shown in Figure (15). The x axis is the controllable variable  $\alpha$ , i.e., the offset in this study. The y axis is the objective  $f$ . The data records all evaluations, i.e., the evaluated  $f$  at a chosen  $\alpha$ . The mean and the standard deviation of the Gaussian process fitting based on the data are also plotted. As one could see, the standard deviation is small around evaluated  $\alpha$ 's while large when there is no nearby evaluated  $\alpha$ 's. The final result suggests that the optimal  $\alpha$  is 4, i.e.,  $\alpha^* = 4$ . With the optimal  $\alpha$ , the optimal value of the objective is around  $-200$ , meaning that with offset as 4, the average travel time of all controllable agents is 200 seconds. Compared with  $\alpha = 0$  and the corresponding average travel time as 220 seconds, the optimal  $\alpha$  could reduce the average travel time by 9%. A much larger  $\alpha$  (i.e.,  $\alpha > 7$ ) may deteriorate the traffic condition and results in a long average travel time.

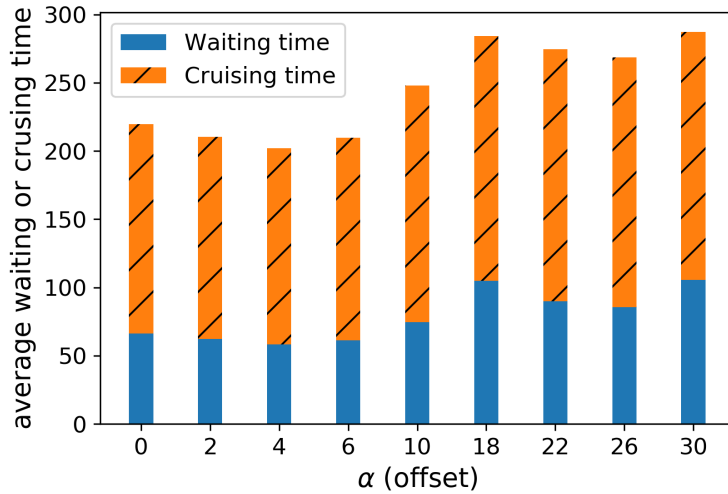


Figure 16: Decomposition of average travel time

To provide more insights, we decompose the average travel time of all controllable agents into two components, namely average waiting time (at intersection) and average cruising time. Both components are presented in Figure (16). In general, a smaller  $\alpha$  (e.g.,  $\alpha < 10$ ) yields a smaller average waiting time and a smaller average cruising time while a larger  $\alpha$  results in a higher average waiting time and a higher cruising time. This could be partially explained as follows. Although the road network is large in the

sense that it has a large number of nodes and links, it covers a relatively small area in Manhattan. The average cruising time from one intersection to an adjacent intersection along the south-north direction is typically around 5 seconds, which is significantly smaller than 10 seconds. With an offset larger than 10 seconds, vehicles have a higher probability of stopping at the next intersection after they stop and wait for green light at the current intersection, resulting in not only a longer accumulative waiting time but also a deteriorated traffic condition. While with a smaller  $\alpha$ , vehicles could take advantage of the “green wave” and enjoy a smaller waiting time and better traffic condition. The lowest waiting time and the lowest cruising time are achieved when the offset is set as 4 seconds, which is exactly the previously derived optimal  $\alpha^*$ .

## 6. Conclusion

This paper develops a unified paradigm that models one’s learning behavior and the system’s equilibrating processes in a routing game among atomic selfish agents. Such a paradigm can assist policymakers in devising optimal operational and planning countermeasures under both normal and abnormal circumstances. A flow-dependent mean field deep Q-learning algorithm is developed to tackle the route choice task of multi-commodity multi-class agents. The flow dependent mean action, which is defined as the traffic flow on the chosen link, carries partial but not full information of nearby agents and is thus able to partially capture the competition among agents. In addition, the use of flow-dependent mean action enables Q-value sharing and policy sharing, which is computationally efficient. The developed algorithm is extensively applied to three road networks, namely a two-node two-link network with CTM as its traffic propagation mechanism (see Section 3), a Braess network with a linear volume delay function (see Section 4), and a large-sized real-world road network with 69 nodes and 166 links implemented in SUMO (see Section 5). The thorough testing unveils the versatility and effectiveness of the developed model-free MARL algorithm.

The linkage between the classic DUE paradigm and our proposed MARL paradigm is then demonstrated in Section 3. On a two-node two link network with CTM as the traffic propagation mechanism, we show that the numerical solution from the developed MARL algorithm agrees well with the solution from an analytical LP formulation in the DSO scenario and the solution from an iterative method in the DUE scenario. To our knowledge, this paper is the first-of-its-kind to unify the mode-based (i.e., DUE) and data-driven (i.e., MARL) paradigms for dynamic routing games.

We demonstrate the effect of two countermeasures, namely tolling (see Section 4) and signal control (see Section 5), on the behavior of travelers and show that the systematic objective of city planners can be optimized by a proper control. The results show that on the Braess network in the study, the optimal toll charge on link  $l_{12}$  is greater or equal to 25, with which the average travel time of selfish agents is minimized and the emergence of Braess paradox could be avoided. In the large-sized real-world road network, the optimal offset for signal control on Broadway is derived as 4 seconds, with which the average travel time of all controllable agents is minimized. The decomposition of travel time into waiting time (at intersections) and cruising time (on the link) further reveals that travelers could take advantage of potential “green wave” when the offset is relatively small (i.e., less than 10 seconds). We note that both the waiting time and cruising time are minimized at the optimal offset, i.e., 4 seconds.

Nevertheless, there are several future directions we would like to explore. First, we assume that all travelers are perfectly rational in this study, meaning that travelers would always take the route with minimal expected travel time. However, bounded rationality (Jayakrishnan et al., 1994; Di et al., 2013) suggests travelers may not switch from their current route to an alternative route with less travel cost if the difference is not large enough. Second, in addition to the route choice, departure time choice is another important research direction. We believe the proposed model-free MARL paradigm is able to accommodate departure time choice of travelers. We leave bounded rationality and the simultaneous route and departure time choice in future research.

## Acknowledgements

This work is partially sponsored by the Region 2 University Transportation Research Center (UTRC) (subcontract RUTGER PO 966112/PID#824227) and the National Science Foundation under CAREER award number CMMI-1943998.

## References

- Bakker, B., Whiteson, S., Kester, L., Groen, F. C. A., 2010. Traffic Light Control by Multiagent Reinforcement Learning Systems. In: Babuška, R., Groen, F. C. A. (Eds.), *Interactive Collaborative Information Systems. Studies in Computational Intelligence*. Springer, Berlin, Heidelberg, pp. 475–510.
- Ban, X. J., Pang, J.-S., Liu, H. X., Ma, R., Mar. 2012a. Continuous-time point-queue models in dynamic network loading. *Transportation Research Part B: Methodological* 46 (3), 360–380.
- Ban, X. J., Pang, J.-S., Liu, H. X., Ma, R., 2012b. Modeling and solving continuous-time instantaneous dynamic user equilibria: A differential complementarity systems approach. *Transportation Research Part B: Methodological* 46 (3), 389–408.
- Bazzan, A. L. C., Grunitzki, R., Jul. 2016. A multiagent reinforcement learning approach to en-route trip building. In: 2016 International Joint Conference on Neural Networks (IJCNN). pp. 5288–5295, iISSN: 2161-4407.
- Bazzan, A. L. C., Klügl, F., 2008. Re-routing Agents in an Abstract Traffic Scenario. In: Zaverucha, G., da Costa, A. L. (Eds.), *Advances in Artificial Intelligence - SBIA 2008. Lecture Notes in Computer Science*. Springer, Berlin, Heidelberg, pp. 63–72.
- Bhalla, S., Ganapathi Subramanian, S., Crowley, M., 2020. Deep Multi Agent Reinforcement Learning for Autonomous Driving. In: Goutte, C., Zhu, X. (Eds.), *Advances in Artificial Intelligence. Lecture Notes in Computer Science*. Springer International Publishing, Cham, pp. 67–78.
- Bliemer, M. C. J., Raadsen, M. P. H., Brederode, L. J. N., Bell, M. G. H., Wismans, L. J. J., Smith, M. J., Jan. 2017. Genetics of traffic assignment models for strategic transport planning. *Transport Reviews* 37 (1), 56–78, publisher: Routledge eprint: <https://doi.org/10.1080/01441647.2016.1207211>.
- Brown, N., Sandholm, T., Jan. 2018. Superhuman AI for heads-up no-limit poker: Libratus beats top professionals. *Science* 359 (6374), 418–424.
- Brown, N., Sandholm, T., Aug. 2019. Superhuman AI for multiplayer poker. *Science* 365 (6456), 885–890.
- Chen, C., Wei, H., Xu, N., Zheng, G., Yang, M., Xiong, Y., Xu, K., Li, Z., Apr. 2020. Toward A Thousand Lights: Decentralized Deep Reinforcement Learning for Large-Scale Traffic Signal Control. *Proceedings of the AAAI Conference on Artificial Intelligence* 34 (04), 3414–3421, number: 04.
- Daganzo, C. F., Aug. 1994. The cell transmission model: A dynamic representation of highway traffic consistent with the hydrodynamic theory. *Transportation Research Part B: Methodological* 28 (4), 269–287.  
URL <http://www.sciencedirect.com/science/article/pii/0191261594900027>
- Daganzo, C. F., Apr. 1995. The cell transmission model, part II: Network traffic. *Transportation Research Part B: Methodological* 29 (2), 79–93.
- de Moraes Ramos, G., Daamen, W., Hoogendoorn, S., 2011. Expected utility theory, prospect theory, and regret theory compared for prediction of route choice behavior. *Transportation Research Record* 2230 (1), 19–28.
- Di, X., Liu, H. X., Mar. 2016. Boundedly rational route choice behavior: A review of models and methodologies. *Transportation Research Part B: Methodological* 85, 142–179.
- Di, X., Liu, H. X., Pang, J.-S., Ban, X. J., Nov. 2013. Boundedly rational user equilibria (BRUE): Mathematical formulation and solution sets. *Transportation Research Part B: Methodological* 57, 300–313.
- Frazier, P. I., Jul. 2018. A Tutorial on Bayesian Optimization. arXiv:1807.02811 [cs, math, stat]ArXiv: 1807.02811.
- Friesz, T. L., Han, K., 2019. The mathematical foundations of dynamic user equilibrium. *Transportation research part B: methodological* 126, 309–328.
- Friesz, T. L., Han, K., Neto, P. A., Meimand, A., Yao, T., 2013. Dynamic user equilibrium based on a hydrodynamic model. *Transportation Research Part B: Methodological* 47, 102–126.
- Friesz, T. L., Luque, J., Tobin, R. L., Wie, B.-W., 1989. Dynamic network traffic assignment considered as a continuous time optimal control problem. *Operations Research* 37 (6), 893–901.
- Gao, S., Frejinger, E., Ben-Akiva, M., 2010. Adaptive route choices in risky traffic networks: A prospect theory approach. *Transportation research part C: emerging technologies* 18 (5), 727–740.
- Gawron, C., May 1998. An Iterative Algorithm to Determine the Dynamic User Equilibrium in a Traffic Simulation Model. *International Journal of Modern Physics C* 09 (03), 393–407, publisher: World Scientific Publishing Co.
- Grunitzki, R., Ramos, G. d. O., Bazzan, A. L. C., Oct. 2014. Individual versus Difference Rewards on Reinforcement Learning for Route Choice. In: 2014 Brazilian Conference on Intelligent Systems. pp. 253–258.
- Hu, H., Liu, H. X., Dec. 2013. Arterial offset optimization using archived high-resolution traffic signal data. *Transportation Research Part C: Emerging Technologies* 37, 131–144.
- Hu, J., Wellman, M. P., Jul. 1998. Multiagent Reinforcement Learning: Theoretical Framework and an Algorithm. In: *Proceedings of the Fifteenth International Conference on Machine Learning. ICML '98*. Morgan Kaufmann Publishers Inc., San Francisco, CA, USA, pp. 242–250.
- Jayakrishnan, R., Mahmassani, H. S., Hu, T.-Y., Sep. 1994. An evaluation tool for advanced traffic information and management systems in urban networks. *Transportation Research Part C: Emerging Technologies* 2 (3), 129–147.
- Kim, G., Ong, Y. S., Cheong, T., Tan, P. S., Aug. 2016. Solving the Dynamic Vehicle Routing Problem Under Traffic Congestion. *IEEE Transactions on Intelligent Transportation Systems* 17 (8), 2367–2380, conference Name: IEEE Transactions on Intelligent Transportation Systems.
- Kumar, S., Shah, P., Hakkani-Tur, D., Heck, L., Dec. 2017. Federated Control with Hierarchical Multi-Agent Deep Reinforcement Learning. arXiv:1712.08266 [cs]ArXiv: 1712.08266.
- Kuwahara, M., Akamatsu, T., Feb. 1997. Decomposition of the reactive dynamic assignments with queues for a many-to-many origin-destination pattern. *Transportation Research Part B: Methodological* 31 (1), 1–10.
- Leibo, J. Z., Zambaldi, V., Lanctot, M., Marecki, J., Graepel, T., Feb. 2017. Multi-agent Reinforcement Learning in Sequential Social Dilemmas. arXiv:1702.03037 [cs]ArXiv: 1702.03037.
- Li, M., Qin, Z., Jiao, Y., Yang, Y., Wang, J., Wang, C., Wu, G., Ye, J., 2019. Efficient Ridesharing Order Dispatching with Mean Field Multi-Agent Reinforcement Learning. In: *The World Wide Web Conference. WWW '19*. ACM, New York, NY, USA, pp. 983–994, event-place: San Francisco, CA, USA.
- Lin, K., Zhao, R., Xu, Z., Zhou, J., 2018. Efficient Large-Scale Fleet Management via Multi-Agent Deep Reinforcement

- Learning. In: Proceedings of the 24th ACM SIGKDD International Conference on Knowledge Discovery & Data Mining. KDD '18. ACM, New York, NY, USA, pp. 1774–1783.
- Littman, M. L., 1994. Markov Games As a Framework for Multi-agent Reinforcement Learning. In: Proceedings of the Eleventh International Conference on International Conference on Machine Learning. ICML'94. Morgan Kaufmann Publishers Inc., San Francisco, CA, USA, pp. 157–163, event-place: New Brunswick, NJ, USA.
- Liu, H. X., He, X., Ban, X., 2007. A Cell-Based Many-to-One Dynamic System Optimal Model and Its Heuristic Solution Method for Emergency Evacuation. Number: 07-2261.  
URL <https://trid.trb.org/view.aspx?id=802113>
- Lowe, R., Wu, Y., Tamar, A., Harb, J., Abbeel, P., Mordatch, I., 2017. Multi-agent Actor-critic for Mixed Cooperative-competitive Environments. In: Proceedings of the 31st International Conference on Neural Information Processing Systems. NIPS'17. Curran Associates Inc., USA, pp. 6382–6393, event-place: Long Beach, California, USA.
- Mao, C., Shen, Z., Aug. 2018. A reinforcement learning framework for the adaptive routing problem in stochastic time-dependent network. *Transportation Research Part C: Emerging Technologies* 93, 179–197.
- Matignon, L., Laurent, G. J., Fort-Piat, N. L., Feb. 2012. Independent reinforcement learners in cooperative Markov games: a survey regarding coordination problems. *The Knowledge Engineering Review* 27 (1), 1–31.
- Merchant, D. K., Nemhauser, G. L., 1978a. A Model and an Algorithm for the Dynamic Traffic Assignment Problems. *Transportation Science* 12 (3), 183–199, publisher: INFORMS.
- Merchant, D. K., Nemhauser, G. L., Aug. 1978b. Optimality Conditions for a Dynamic Traffic Assignment Model. *Transportation Science* 12 (3), 200–207, publisher: INFORMS.
- Mnih, V., Kavukcuoglu, K., Silver, D., Rusu, A. A., Veness, J., Bellemare, M. G., Graves, A., Riedmiller, M., Fidjeland, A. K., Ostrovski, G., Petersen, S., Beattie, C., Sadik, A., Antonoglou, I., King, H., Kumaran, D., Wierstra, D., Legg, S., Hassabis, D., Feb. 2015. Human-level control through deep reinforcement learning. *Nature* 518 (7540), 529–533.
- Nguyen, T. T., Nguyen, N. D., Nahavandi, S., Dec. 2018. Deep Reinforcement Learning for Multi-Agent Systems: A Review of Challenges, Solutions and Applications. arXiv:1812.11794 [cs, stat]ArXiv: 1812.11794.
- Nguyen, T. T., Nguyen, N. D., Nahavandi, S., Sep. 2020. Deep Reinforcement Learning for Multiagent Systems: A Review of Challenges, Solutions, and Applications. *IEEE Transactions on Cybernetics* 50 (9), 3826–3839, conference Name: IEEE Transactions on Cybernetics.
- Nie, X., Zhang, H. M., 2005. A comparative study of some macroscopic link models used in dynamic traffic assignment. *Networks and Spatial Economics* 5 (1), 89–115.
- OpenAI, 2018. Openai five. <https://blog.openai.com/openai-five/>.
- Palanisamy, P., Nov. 2019. Multi-Agent Connected Autonomous Driving using Deep Reinforcement Learning. arXiv:1911.04175 [cs, stat]ArXiv: 1911.04175.
- Pas, E. I., Principio, S. L., Jun. 1997. Braess' paradox: Some new insights. *Transportation Research Part B: Methodological* 31 (3), 265–276.
- Peeta, S., Zhou, C., Oct. 1999. Robustness of the off-line a priori stochastic dynamic traffic assignment solution for on-line operations. *Transportation Research Part C: Emerging Technologies* 7 (5), 281–303.
- Peeta, S., Ziliaskopoulos, A. K., 2001. Foundations of dynamic traffic assignment: The past, the present and the future. *Networks and spatial economics* 1 (3-4), 233–265.
- Prasad, A., Dusparic, I., Sep. 2019. Multi-agent Deep Reinforcement Learning for Zero Energy Communities. In: 2019 IEEE PES Innovative Smart Grid Technologies Europe (ISGT-Europe). pp. 1–5.
- Puterman, M. L., 1994. Markov Decision Processes: Discrete Stochastic Dynamic Programming, 1st Edition. John Wiley & Sons, Inc., New York, NY, USA.
- Ramos, G. d. O., Bazzan, A. L. C., da Silva, B. C., Mar. 2018. Analysing the impact of travel information for minimising the regret of route choice. *Transportation Research Part C: Emerging Technologies* 88, 257–271.
- Seongmoon Kim, Lewis, M. E., White, C. C., Jun. 2005. Optimal vehicle routing with real-time traffic information. *IEEE Transactions on Intelligent Transportation Systems* 6 (2), 178–188, conference Name: IEEE Transactions on Intelligent Transportation Systems.
- Shou, Z., Di, X., Feb. 2020. Reward Design for Driver Repositioning Using Multi-Agent Reinforcement Learning. arXiv:2002.06723 [cs, stat]ArXiv: 2002.06723.
- Shou, Z., Di, X., Ye, J., Zhu, H., Zhang, H., Hampshire, R., Feb. 2020. Optimal passenger-seeking policies on E-hailing platforms using Markov decision process and imitation learning. *Transportation Research Part C: Emerging Technologies* 111, 91–113.
- Silver, D., Huang, A., Maddison, C. J., Guez, A., Sifre, L., van den Driessche, G., Schrittwieser, J., Antonoglou, I., Panneershelvam, V., Lanctot, M., Dieleman, S., Grewe, D., Nham, J., Kalchbrenner, N., Sutskever, I., Lillicrap, T., Leach, M., Kavukcuoglu, K., Graepel, T., Hassabis, D., Jan. 2016. Mastering the game of Go with deep neural networks and tree search. *Nature* 529 (7587), 484–489.
- Silver, D., Schrittwieser, J., Simonyan, K., Antonoglou, I., Huang, A., Guez, A., Hubert, T., Baker, L., Lai, M., Bolton, A., Chen, Y., Lillicrap, T., Hui, F., Sifre, L., van den Driessche, G., Graepel, T., Hassabis, D., Oct. 2017. Mastering the game of Go without human knowledge. *Nature* 550 (7676), 354–359.
- Srinivas, N., Krause, A., Kakade, S., Seeger, M., Jun. 2010. Gaussian process optimization in the bandit setting: no regret and experimental design. In: Proceedings of the 27th International Conference on International Conference on Machine Learning. ICML'10. Omnipress, Haifa, Israel, pp. 1015–1022.
- Stefanello, F., Silva, B. C. d., Bazzan, A. L. C., 2016. Using Topological Statistics to Bias and Accelerate Route Choice: Preliminary Findings in Synthetic and Real-World Road Networks. In: ATT@IJCAI.
- Steinberg, R., Zangwill, W. I., Aug. 1983. The Prevalence of Braess' Paradox. *Transportation Science* 17 (3), 301–318, publisher: INFORMS.
- Sumalee, A., Zhong, R. X., Pan, T. L., Szeto, W. Y., Mar. 2011. Stochastic cell transmission model (SCTM): A stochastic dynamic traffic model for traffic state surveillance and assignment. *Transportation Research Part B: Methodological* 45 (3), 507–533.
- Sutton, R. S., Barto, A. G., 1998. Introduction to Reinforcement Learning, 1st Edition. MIT Press, Cambridge, MA, USA.
- Vinyals, O., Babuschkin, I., Czarnecki, W. M., Mathieu, M., Dudzik, A., Chung, J., Choi, D. H., Powell, R., Ewalds, T.,



- Georgiev, P., Oh, J., Horgan, D., Kroiss, M., Danihelka, I., Huang, A., Sifre, L., Cai, T., Agapiou, J. P., Jaderberg, M., Vezhnevets, A. S., Leblond, R., Pohlen, T., Dalibard, V., Budden, D., Sulsky, Y., Molloy, J., Paine, T. L., Gulcehre, C., Wang, Z., Pfaff, T., Wu, Y., Ring, R., Yogatama, D., Wünsch, D., McKinney, K., Smith, O., Schaul, T., Lillicrap, T., Kavukcuoglu, K., Hassabis, D., Apps, C., Silver, D., Nov. 2019. Grandmaster level in StarCraft II using multi-agent reinforcement learning. *Nature* 575 (7782), 350–354.
- Waller, S. T., Ziliaskopoulos, A. K., Jan. 2001. Stochastic Dynamic Network Design Problem. *Transportation Research Record* 1771 (1), 106–113, publisher: SAGE Publications Inc.
- Xu, H., Lou, Y., Yin, Y., Zhou, J., 2011. A prospect-based user equilibrium model with endogenous reference points and its application in congestion pricing. *Transportation Research Part B: Methodological* 45 (2), 311–328.
- Yang, J., Jiang, G., 2014. Development of an enhanced route choice model based on cumulative prospect theory. *Transportation Research Part C: Emerging Technologies* 47, 168–178.
- Yang, Y., Luo, R., Li, M., Zhou, M., Zhang, W., Wang, J., Jul. 2018. Mean Field Multi-Agent Reinforcement Learning. In: *International Conference on Machine Learning*. pp. 5571–5580.
- Yu, Y., Han, K., Ochieng, W., May 2020. Day-to-day dynamic traffic assignment with imperfect information, bounded rationality and information sharing. *Transportation Research Part C: Emerging Technologies* 114, 59–83.
- Zhang, C., Liu, T.-L., Huang, H.-J., Chen, J., 2018. A cumulative prospect theory approach to commuters’ day-to-day route-choice modeling with friends’ travel information. *Transportation Research Part C: Emerging Technologies* 86, 527–548.
- Zhou, B., Song, Q., Zhao, Z., Liu, T., Apr. 2020. A reinforcement learning scheme for the equilibrium of the in-vehicle route choice problem based on congestion game. *Applied Mathematics and Computation* 371, 124895.
- Ziliaskopoulos, A. K., Feb. 2000. A Linear Programming Model for the Single Destination System Optimum Dynamic Traffic Assignment Problem. *Transportation Science* 34 (1), 37–49, publisher: INFORMS.